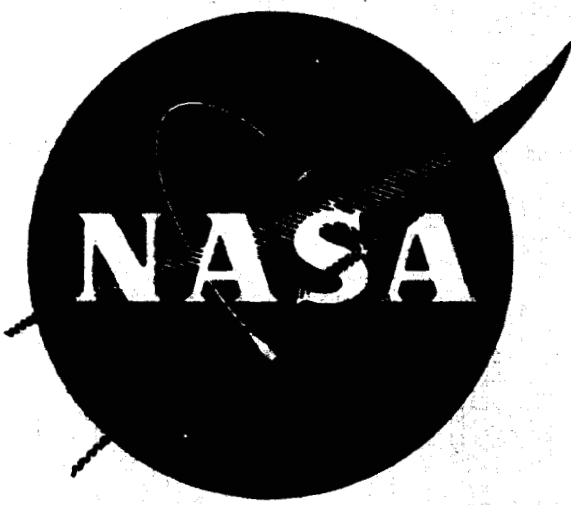


WANL-PR(P)-007  
NASA CR-54434



# DETERMINATION OF THE WELDABILITY AND ELEVATED TEMPERATURE STABILITY OF REFRACTORY METAL ALLOYS

Seventh Quarterly Report

by

G. G. Lessmann and D. R. Stoner

prepared for

National Aeronautics and Space Administration

Lewis Research Center

Space Power Systems Division

Under Contract NAS 3-2540



**Astronuclear Laboratory**  
**Westinghouse Electric Corporation**

(THRU) \_\_\_\_\_  
 (CODE) \_\_\_\_\_  
 (CATEGORY) \_\_\_\_\_

N65-31176  
 (ACCESSION NUMBER)

59  
 (PAGES)

03-54434  
 (NASA CR OR TMX OR AD NUMBER)

FACILITY FORM 602

GPO PRICE \$ \_\_\_\_\_

CFSTI PRICE(S) \$ 3.10

Hard copy (HC) \$ 10.50

Microfiche (MF) \$ 10.50

## NOTICE

This report was prepared as an account of Government-sponsored work. Neither the United States nor the National Aeronautics and Space Administration (NASA), nor any person acting on behalf of NASA:

- A) Makes any warranty or representation, expressed or implied, with respect to the accuracy, completeness, or usefulness of the information contained in this report, or that the use of any information, apparatus, method, or process disclosed in this report may not infringe privately-owned rights; or
- B) Assumes any liabilities with respect to the use of, or for damages resulting from the use of any information, apparatus, method or process disclosed in this report.

As used above, "person acting on behalf of NASA" includes any employee or contractor of NASA, or employee of such contractor, to the extent that such employee or contractor of NASA or employee of such contractor prepares, disseminates, or provides access to, any information pursuant to his employment or contract with NASA, or his employment with such contractor.

**CASE FILE**

**DETERMINATION OF THE WELDABILITY AND ELEVATED  
TEMPERATURE STABILITY OF REFRACTORY METAL ALLOYS**

by

G. G. Lessmann

and

D. R. Stoner

**Seventh Quarterly Report**

Covering the Period

December 21, 1964 to March 20, 1965

Prepared for

**NATIONAL AERONAUTICS AND SPACE ADMINISTRATION  
Contract NAS 3-2540**Technical Management  
Paul E. Moorhead  
NASA - Lewis Research Center  
Space Power Systems Div.Astronuclear Laboratory  
Westinghouse Electric Corporation  
Pittsburgh 36, Pa.

## FOREWORD

This report describes work accomplished under Contract NAS 3-2540 during the period December 21, 1964 to March 20, 1965. This program is being administered by R. T. Begley of the Astronuclear Laboratory, Westinghouse Electric Corporation. G. G. Lessmann and D. R. Stoner performed the experimental investigations.

Mr. P. E. Moorhead of the National Aeronautics and Space Administration is Technical Manager of this program.

## TABLE OF CONTENTS

	<u>Page</u>
I INTRODUCTION	1
II SUMMARY	3
III TECHNICAL PROGRAM	5
A. WELDING EVALUATIONS	5
1. TIG Weld Contamination	5
2. Post Weld Annealing Studies	9
B. THERMAL STABILITY SCREEN OF FS-85, T-111, and T-222 WELDS	23
C. EFFECT OF CONTAMINATION ON THE WELDABILITY OF REFRACTORY METAL ALLOYS	34
IV FUTURE WORK	50
V REFERENCES	51

LIST OF FIGURES

	<u>Page</u>
1. Interstitial Contaminant Absorption Showing a Random Distribution of Columbium and Tantalum Alloy TIG Welds	7
2. Normal Distribution Plot for Weld Contamination Analyses	8
3. Summary Showing the Effect of Annealing on TIG Weld Bend Ductility	12
4. Summary Showing the Effect of Annealing on EB Weld Bend Ductility	13
5. Effect of Post Weld Annealing on B-66 Weld Ductility	14
6. Effect of Post Weld Annealing on C-129Y Weld Ductility	15
7. Effect of Post Weld Annealing on Cb-752 Weld Ductility	16
8. Effect of Post Weld Annealing on D-43 Weld Ductility	17
9. Effect of Post Weld Annealing on FS-85 Weld Ductility	18
10. Effect of Post Weld Annealing on SCb-291 Weld Ductility	19
11. Effect of Post Weld Annealing on T-111 Weld Ductility	20
12. Effect of Post Weld Annealing on T-222 Weld Ductility	21
13. Effect of Post Weld Annealing on Ta-10W Weld Ductility	22
14. Effect of Aging at 1800°F on Welded FS-85	24
15. Effect of Aging at 1800°F on Welded T-111	25
16. Effect of Aging at 1800°F on Welded T-222	26
17. Effect of Aging at 1800°F on FS-85, T-111 and T-222 TIG Welds	27
18. Microstructure of FS-85 TIG Welds	28
19. Weld and Heat Affected Zone Microstructures of T-111 TIG Weld	30
20. Heat Affected Zone-Base Metal Area Microstructure of T-111 TIG Welds	31

LIST OF FIGURES (Continued)

	<u>Page</u>
21. Vapor Deposit Shadowing Effect Observed on Adjacent Specimens Annealed 1000 Hours at 1800°F. Arrows Indicate Specimen From Which, and Specimen onto Which Shadows were Thrown	35
22. Vapor Deposit Shadowing Effect Observed on Adjacent Specimens Annealed 1000 Hours at 1800°F. Arrows Indicate Specimen from Which, and Specimen onto Which Shadows Were Thrown	36
23. Program Outline for Contaminated Alloy Weldability Evaluation	38
24. Schematic of Oxygen Doping Apparatus	39
25. Oxygen Doping Furnace Fixture	40
26. Oxygen Doping Furnace and Gas Handling Equipment	41
27. Relationship of Doping Variables and Depletion of Oxygen in the Helium Carrier Gas	43
28. Process Correction Curve Based on Observed 1500°F Oxidation Rate (Using 100 ppm Oxygen Doped Helium at 100 cc/min Flow Rate)	44
29. FS-85 Doped to 750 ppm Oxygen (Prior to Diffusion Heat Treatment)	45
30. Bend Ductility as a Function of Oxygen Content	46

LIST OF TABLES

	<u>Page No.</u>
1. Alloys Included in the Weldability and Thermal Stability Evaluations	2
2. Results of TIG Weld Interstitial Chemistry	6
3. Optimized Weld Parameters	10
4. Recommended One Hour Post Weld Anneals	11
5. Selected Oxygen Contamination Levels	48



## I. INTRODUCTION

This is the Seventh Quarterly Progress Report describing work accomplished under Contract NAS 3-2540. The objective of this program is to determine the weldability and long time elevated temperature stability of promising refractory metal alloys in order to determine those most suitable for use in advanced alkali-metal space electric power systems. A detailed discussion of the program and program objectives was presented in the First Quarterly Report. Alloys included in this investigation are listed in Table 1.

Process and test controls employed throughout this program emphasize the important influence of interstitial elements on the properties of refractory metal alloys. Stringent process and test procedures are required, including continuous monitoring of the TIG weld chamber atmosphere, electron beam welding at low pressures, aging in furnaces employing hydrocarbon free pumping systems providing pressures less than  $10^{-8}$  torr, and chemical sampling following successive stages of the evaluation for verification of these process controls.

Equipment requirements and set-up, and procedures for welding and testing, have been described in previous progress reports. Any improvements in processes, changes in procedures, or additional processes and procedures are described in this report.

**TABLE 1 - Alloys Included in the Weldability and Thermal Stability Evaluations**

<u>Alloy</u>	<u>Nominal Composition Weight Percent</u>
AS-55	Cb-5W-1Zr-0.2Y-0.06C
B-66	Cb-5Mo-5V-1Zr
C-129Y	Cb-10W-10Hf+Y
Cb-752	Cb-10W-2.5Zr
D-43	Cb-10W-1Zr-0.1C
FS-85	Cb-27Ta-10W-1Zr
SCb-291	Cb-10W-10Ta
D43 + Y	Cb-10W-1Zr-0.1C+Y
T-111	Ta-8W-2Hf
T-222	Ta-9.6W-2.4Hf-0.01C
Ta-10W	Ta-10W
W-25 Re	W-25Re
W	Unalloyed
Sylvania "A"	W-0.5Hf-0.02C

**NOTE: All alloys from arc-cast and/or electron beam melted material except Sylvania "A"**

## II. SUMMARY

The remainder of the material required for this program was received during this period. In addition to the alloys listed in Table 1, a limited quantity of yttrium modified Cb-10W-1Zr-0.1C sheet was procured from Wah Chang. The purpose in evaluating this material is to determine if yttrium would be beneficial in improving D-43 weld ductility in a manner similar to that observed with C-129Y and AS-55. The weldability evaluation of this material is nearly complete and will be reported in the next quarterly report.

The post weld annealing series were completed for the tantalum and columbium alloys with the exception of yttrium modified D43. Since testing at numerous temperature-time combinations is impractical, three one-hour post weld annealing temperatures in the stress relief-recrystallization range were chosen. For the columbium alloys these were 1900°F, 2200°F and 2400°F and for the tantalum alloys 2400°F, 2700°F and 3000°F. The purpose of these tests was twofold: to screen for short time thermal instabilities (i.e. aging) and to identify an overaged state for pretreatment in the final phase of this program, the long time thermal stability studies. Ductility as measured by the bend ductile-to-brittle transition temperature was used to measure weld response to annealing. After EB or TIG welding and annealing, the tantalum alloys remained ductile to the lowest test temperature, -320°F, except T-222 TIG welds annealed at 2700°F which had a slightly raised DBTT of -250°F. TIG welds in columbium alloys responded to annealing with varying degrees of severity by losing ductility at the lower annealing temperatures and showing improvement over the as-welded ductility after annealing at the higher temperature, 2400°F. Hence, these displayed an age-overage response with increasing annealing temperatures demonstrating the need for post weld annealing in these systems. TIG welds in B-66 were not typical in this respect since, while failing to overage, they lost ductility slowly with increasing annealing temperatures. Except for Cb-752, EB welds in the columbium alloys showed improved ductility with annealing but did not display an age-overage behavior. Cb-752 EB welds responded by aging and overaging as was typical of the TIG welds.

Chemical analysis data for carbon, oxygen, and nitrogen pick-up in eighteen TIG welds were obtained and reviewed. No apparent contamination occurred during welding.

The thermal stability study welds for the columbium and tantalum alloys were completed, inspected, and are being machined to the required bend and tensile test configurations.

An evaluation of the effect of oxygen contamination on the weldability of T-111, T-222, and FS-85 was initiated as an addition to this contract. Preliminary data were developed. The results seem to discriminate substantially between the ductility of T-111 and T-222 at the 150-200 ppm oxygen level. This is quite surprising and requires further verification. The detailed objectives of this effort are described in this report. The rate of oxidation of FS-85 in oxygen doped helium proved to be about equal to the oxidation rate reported for Cb-1Zr in vacuum at an oxygen partial pressure three orders of magnitude lower than used for FS-85. Hence, the inert environment appears to offer an additional shielding advantage as compared to a simple vacuum.

Welds in T-111, T-222, and FS-85 were screened for thermal stability at 1800°F. All responded to aging with a measureable rise in the bend ductile-brittle transition temperature. Hardness traverses proved useful for following the aging responses. During the  $10^{-10}$  torr aging runs of 100 and 1000 hours, specimen staining occurred as a result of vapor transfer of hafnium and zirconium.

### III. TECHNICAL PROGRAM

#### A. WELDING EVALUATIONS

1. TIG Weld Contamination - A representative sample of welds in 0.035 inch sheet was analyzed for carbon, oxygen, and nitrogen pick-up. Two welds from each of six columbium alloys and three tantalum alloys were included. Specimens selected from each alloy were those welded in the best and poorest quality atmosphere. The results are listed in Table 2 along with the base metal chemistry. This data is plotted in Figure 1. No correlation is apparent between change in interstitial levels and atmosphere quality with points seemingly grouped randomly. This observation is borne out by Figure 2 in which the same data is shown plotted on a normal distribution probability scale. Random variation appears to be associated with the values obtained. Carbon and nitrogen values deviate from the normal distribution behavior (a straight line on this plot) and show a slight mean contamination value for the weld as compared with base metal. However, the no contamination (zero) points for these lie within the 95% confidence limits implying that little or no carbon and nitrogen contamination has occurred. The two high changes in carbon level (-100 ppm) were recorded for D-43 and are therefore not as much out of line as would appear on Figures 1 and 2 since this change is within 10% of the intentional 0.1% carbon alloying level.

The oxygen data represent a very nearly normal distribution and display a definite bias indicating a loss of this element during welding in the high purity helium atmosphere of between 15.6 and 39.4 ppm. This bias in oxygen analyses could be real or superficial. Additional experience in this area is anticipated and should serve to clarify these results. These observations show clearly that individual chemical analyses are not sufficiently accurate, and that a reasonable size statistic sample is required to demonstrate the adequacy of weld atmosphere control.

Oxygen analyses of these samples were obtained by the vacuum fusion technique, nitrogen by the Kjeldahl technique, and carbon using a combustion technique with a conductometric finish. These analyses were performed under the direction of Dr. O. H. Kriege, Westinghouse Research and Development Center.

**TABLE 2 - Results of TIG Weld Interstitial Chemistry**

Alloy	Specimen No.	Weld No.	Atmosphere Monitor Readings (ppm)			Base Metal Chemistry			Weld Chemistry and Change From Base					
			O <sub>2</sub> (1)	O <sub>2</sub> (2)	H <sub>2</sub> O (3)	O-ppm.	N-ppm	C-ppm	O	ΔO	N	ΔN	C	ΔC
B-66	C <sub>1</sub> -G <sub>2</sub> H <sub>2</sub>	8	0.3	2.4	0.1	150	30	44	130	-20	53	+23	49	+5
B-66	C <sub>1</sub> -A <sub>2</sub> B <sub>2</sub>	3	5.0	5.4	0.05	150	30	44	110	-40	76	+46	41	-3
D-43	C <sub>2</sub> -G <sub>3</sub> H <sub>3</sub>	6	4.0	4.6	2.4	180	10	1100	110	-70	45	+35	1000	-100
D-43	C <sub>2</sub> -1 <sub>1</sub> J <sub>1</sub>	9	0.5	2.2	0.3	180	10	1100	120	-60	31	+21	1000	-100
FS-85	C3-G <sub>2</sub> H <sub>2</sub>	7	2.2	4.6	2.5	98	50	12	75	-23	37	-13	15	+3
FS-85	C3-A <sub>2</sub> B <sub>2</sub>	3	4.0	6.2	0.5	98	50	12	72	-26	45	-5	13	+1
Cb-752	C4-1 <sub>2</sub> J <sub>2</sub>	6	--	3.2	0.5	180	80	21	130	-50	65	-15	29	+8
Cb-752	C4-G <sub>1</sub> H <sub>1</sub>	8	--	2.8	0.05	180	80	21	150	-30	102	+22	47	+26
SCb-291	C5-1 <sub>3</sub> J <sub>3</sub>	3	2.5	3.6	0.4	110	50	17	100	-10	63	+13	14	-3
SCb-291	C5-A <sub>2</sub> B <sub>2</sub>	9	0.5	2.1	0.2	110	50	17	73	-37	38	-12	21	+4
C-129Y	CG-C <sub>1</sub> D <sub>1</sub>	2	3.5	--	0.9	102	60	36	58	-44	50	-10	47	+11
C-129Y	C <sub>6</sub> -E <sub>3</sub> F <sub>3</sub>	9	0.5	2.1	0.3	102	60	36	46	-56	29	-31	39	+3
T-111	Ti-B <sub>1</sub> B <sub>2</sub>	1	1.5	3	0.5	15	18	48	24	+9	29	+11	28	-20
T-111	Ti-B <sub>1</sub> B <sub>9</sub>	10	0.5	4	1.6	15	18	48	24	+9	23	+5	39	-9
T-222	T3-A <sub>1</sub> A <sub>2</sub>	1	--	1.5	0.3	29	<10	100	22	-7	18	+8	130	+30
T-222	T3-B <sub>1</sub> B <sub>11</sub> <sup>12</sup>	12	--	2.5	2.4	29	<10	100	22	-7	14	+4	120	+20
Ta-10W	T2-G <sub>2</sub> H <sub>2</sub>	8	0.0	2.7	0.15	66	100	12	40	-26	8	-92	13	+1
Ta-10W	T2-J <sub>1</sub> J <sub>1</sub>	6	5.0	4.0	5.2	66	100	12	59	-7	7	-93	10	+2

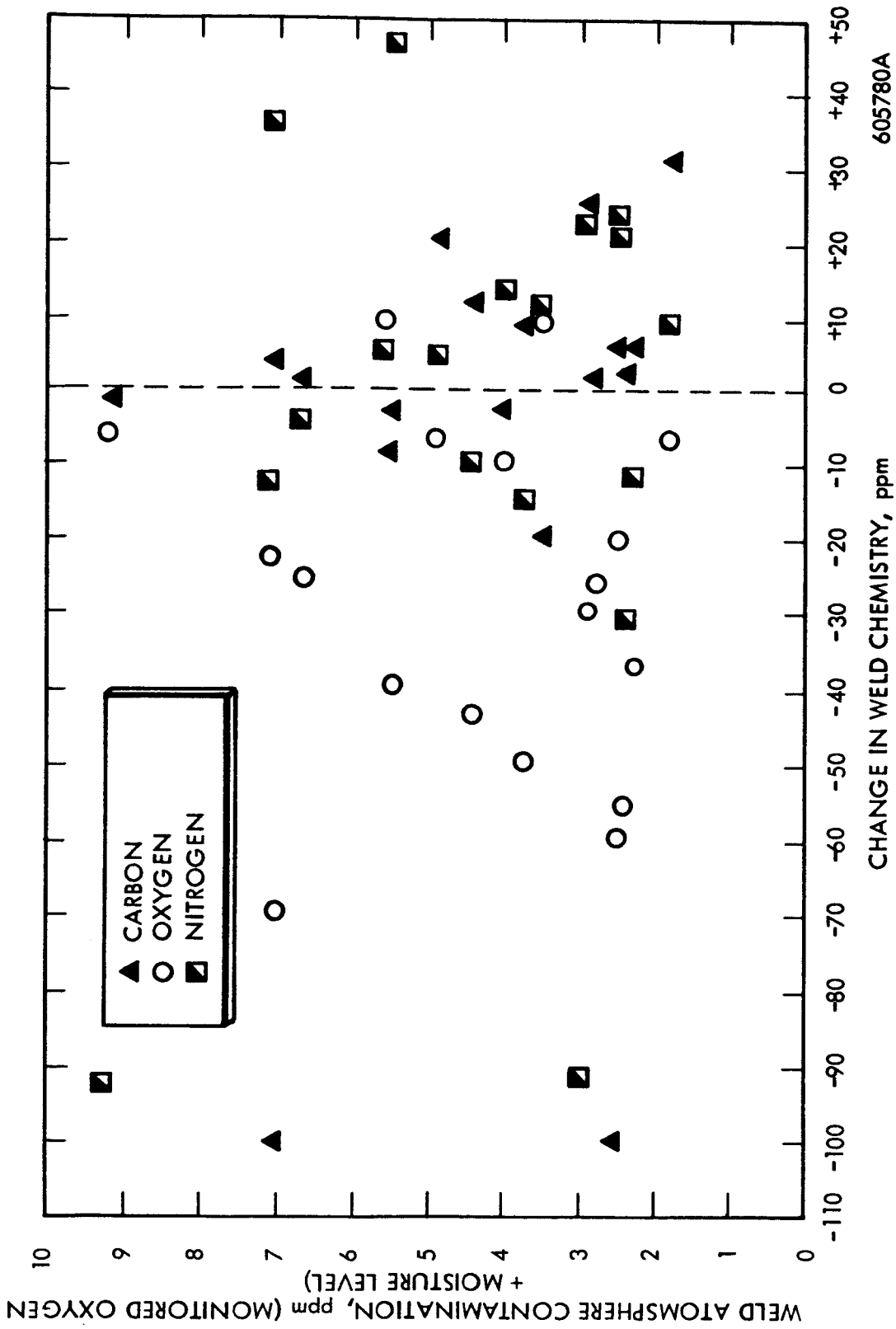


FIGURE 1 - Interstitial Contaminant Absorption Showing a Random Distribution of Columbium and Tantalum Alloy TIG Welds

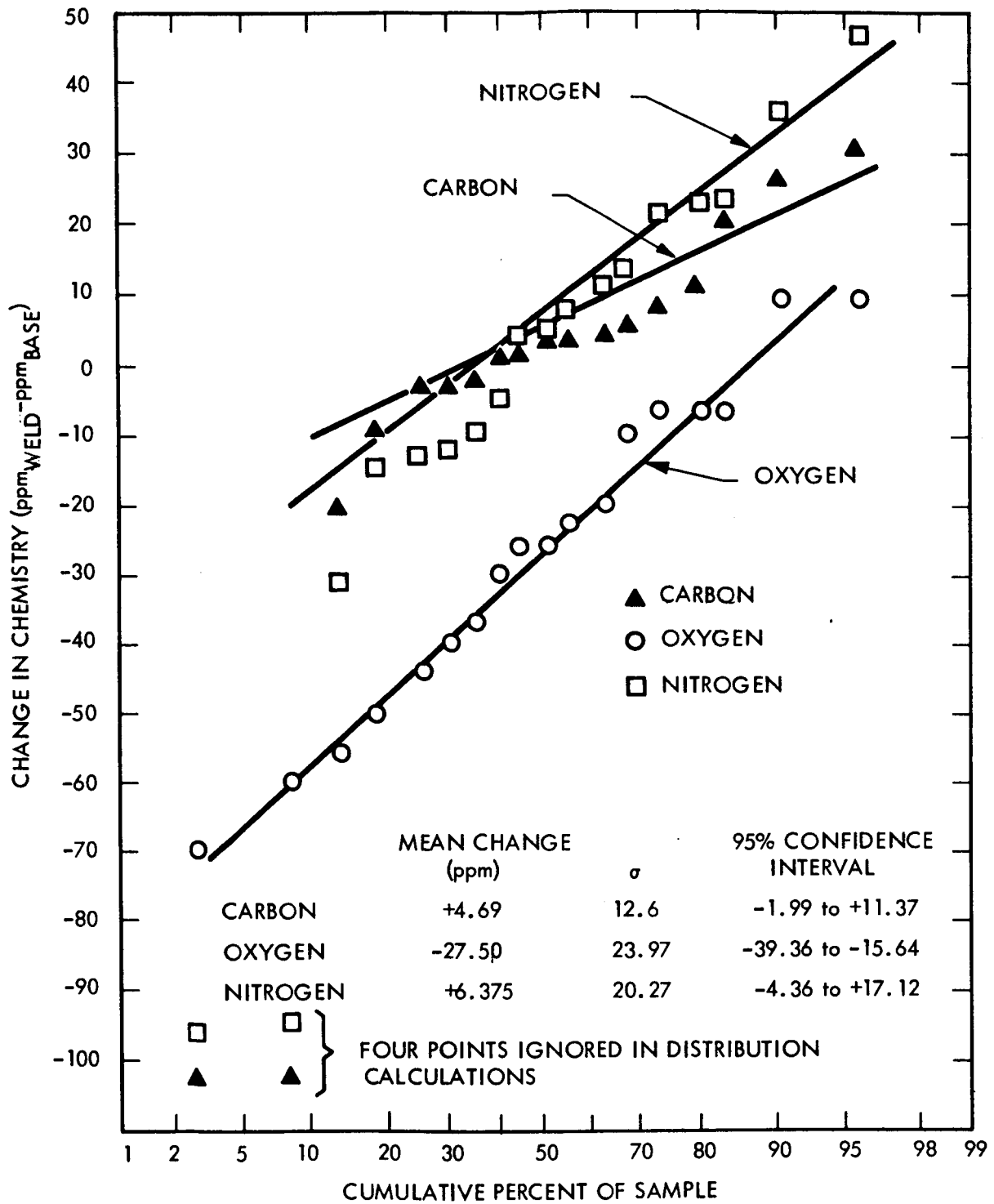


FIGURE 2 - Normal Distribution Plot for Weld Contamination Analyses



2. Post Weld Annealing Studies - Post weld annealing studies were completed for six columbium base alloys and three tantalum base alloys. Annealing effects were evaluated on the basis of the observed shift in bend ductile-to-brittle transition temperature as a function of annealing temperature. TIG weld results for all the alloys are summarized in Figure 3, and EB weld results in Figure 4. Only longitudinal bend test results are plotted in these figures. Transverse bend test results are included in Figures 5 to 13 in which the post weld annealing responses are plotted individually for the various alloys. The 144 bend transition curves which are summarized in these figures are not included in this report.

One hour post weld annealing temperatures were selected in the stress relief-recrystallization range. Hence, the columbium alloys were annealed at 1900°F, 2200°F, and 2400°F, while the tantalum alloys were annealed at 2400°F, 2700°F, and 3000°F. Welding parameters which produced the lowest as-welded DBTT, as determined during the previously reported parameter optimization series, were used in preparing welds for this evaluation. These are listed in Table 3. The optimized weld parameters in combination with the most beneficial post weld anneal, if any, will be used for preparation and conditioning of specimens for evaluation in the thermal stability phase of this program. This approach is expected to provide a metallurgical structure optimized with respect to thermal stability prior to conducting long time aging tests. Selected post weld anneals are listed in Table 4.

All of the columbium alloys responded to post weld annealing. TIG welds in D-43, Cb-752, C-129Y, and SCb-291 appear to experience an age-overage response. FS-85 TIG welds experience improved ductility after the 1900°F anneal, secondary aging during the 2200°F anneal and overaging at 2400°F. A similar response in FS-85 has been reported previously<sup>(1)</sup>. B-66 showed a 50°F increase in DBTT probably resulting primarily from grain growth. Except for T-222 at 2700°F, the TIG welded tantalum alloys did not respond to annealing with any apparent change in the bend transition temperature.

Among the EB welds only Cb-752 displayed an age-overage reaction. The other columbium alloys demonstrated improved ductility with annealing while the tantalum alloys and SCb-291 EB welds were ductile below -320°F for all conditions.

**TABLE 3 - Optimized Weld Parameters**

Alloy	TIG WELDS				EB WELDS				
	Speed (ipm)	Clamp Spacing (in.)	Current Amps (DCSP)	Arc Gap (in.)	Speed (ipm)	Clamp Spacing (in.)	Deflection (in.) <sup>(1)</sup>	Voltage (KV)	Current (ma)
AS-55	---	---	---	0.06	25	3/16	0.050	150	3.6
B-66	15	3/8	86	0.06	25	3/16	0.050	150	3.2
C-129Y	30	3/8	110	0.06	50	1/2	0.050	150	4.1
Cb-752	30	3/8	87	0.06	15	3/16	0.050	150	3.3
D-43	30	3/8	114	0.06	50	1/2	0.050	150	4.4
FS-85	15	3/8	90	0.06	50	3/16	0.050	150	4.4
SCb-291	15	1/4	83	0.06	50	1/2	0.050	150	4.4
T-111	15	3/8	115	0.06	15	1/2	0.050	150	3.8
T-222	30	1/4	190	0.06	15	1/2	0.050	150	4.5
Ta-10W	7.5	1/4	118	0.06	15	1/2	0.050	150	3.8

(1) Beam deflection at 60 $\sim$  parallel to weld direction.

**TABLE 4 - Recommended One Hour Post Weld Anneals  
(Selected for Pre-Treatment of Welds  
for the Thermal Stability Study)**

<u>Alloy</u>	<u>TIG Welds</u>	<u>EB Welds</u>
B-66	None	1900°F
D-43	2400°F	2400°F
FS-85	2400°F	2200°F
Cb-752	2200°F	2400°F
SCb-291	2200°F	None
C-129Y	2400°F	2200°F
T-111	2400°F	2400°F
Ta-10W	None	None
T-222	2400°F	2400°F

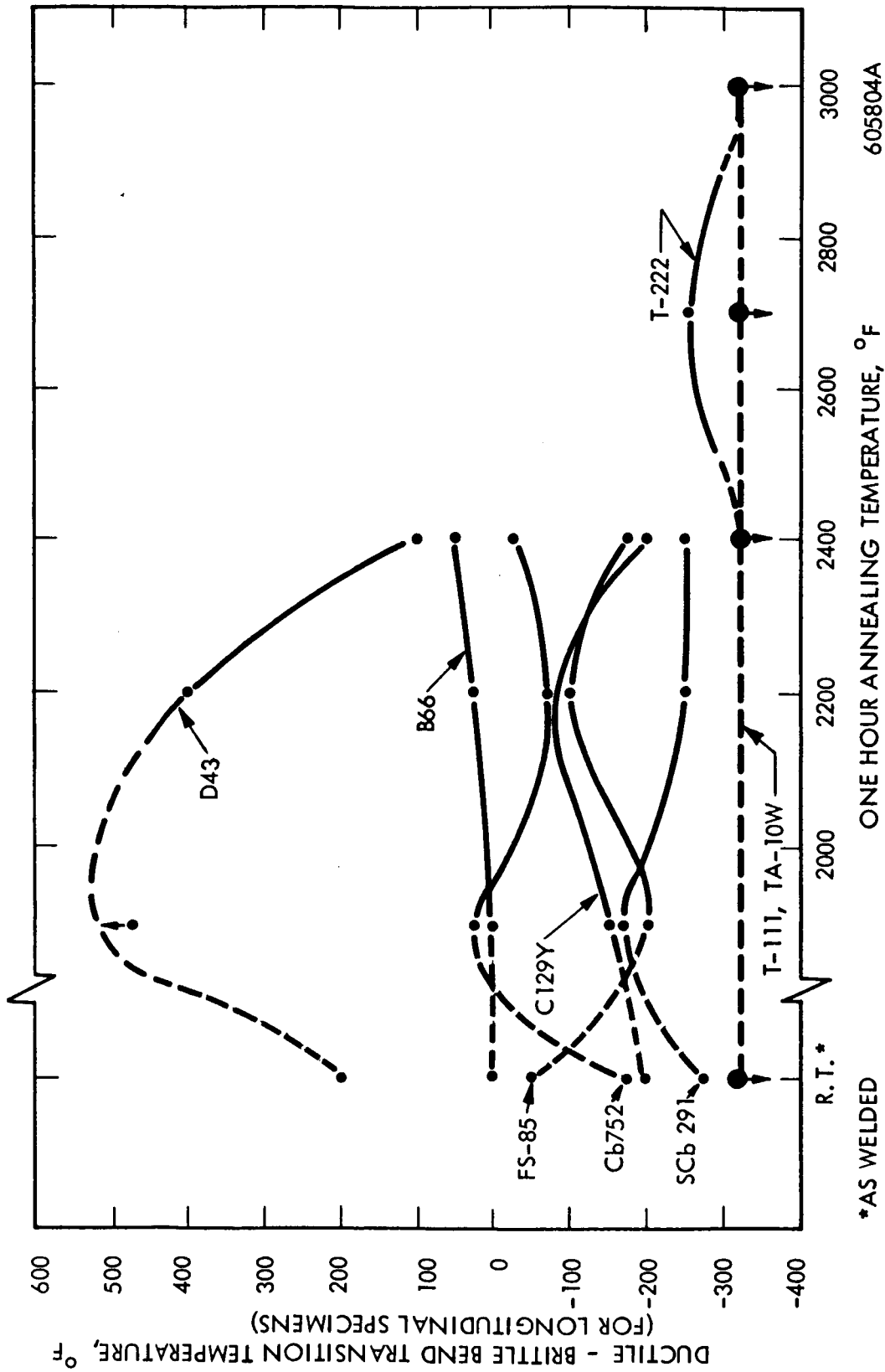


FIGURE 3 - Summary Showing the Effect of Annealing on TIG Weld Bend Ductility

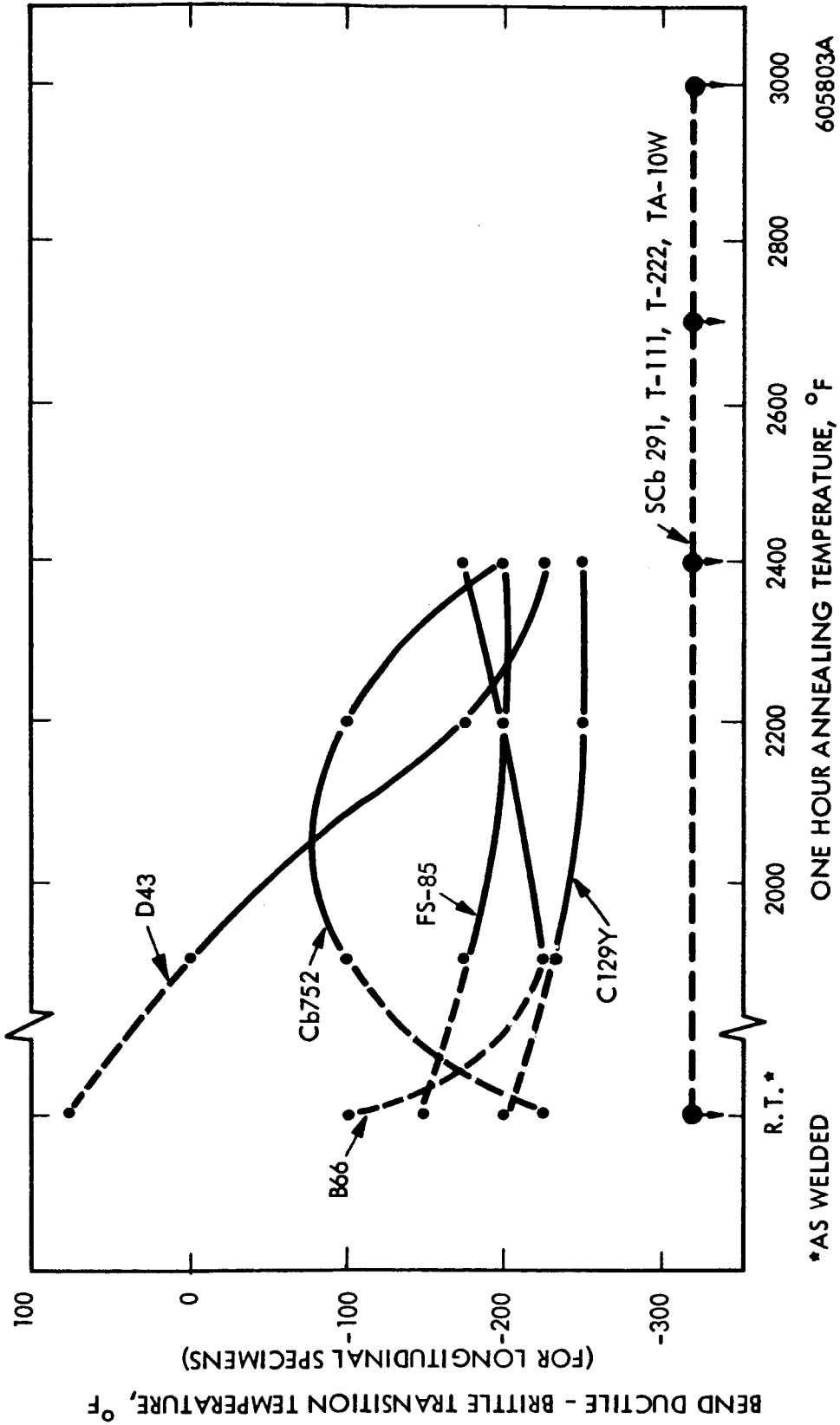


FIGURE 4 - Summary Showing the Effect of Annealing on EB Weld Bend Ductility

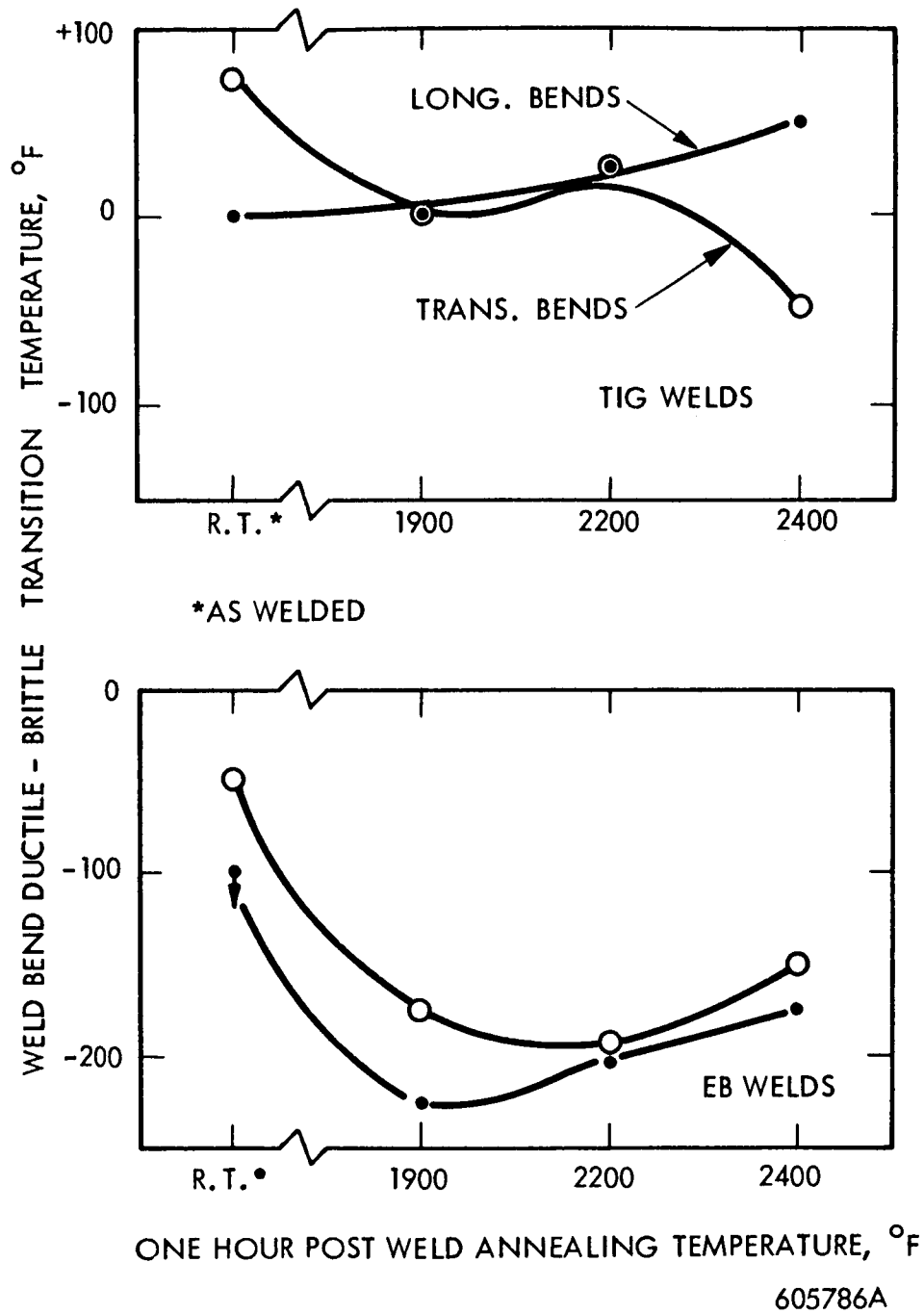
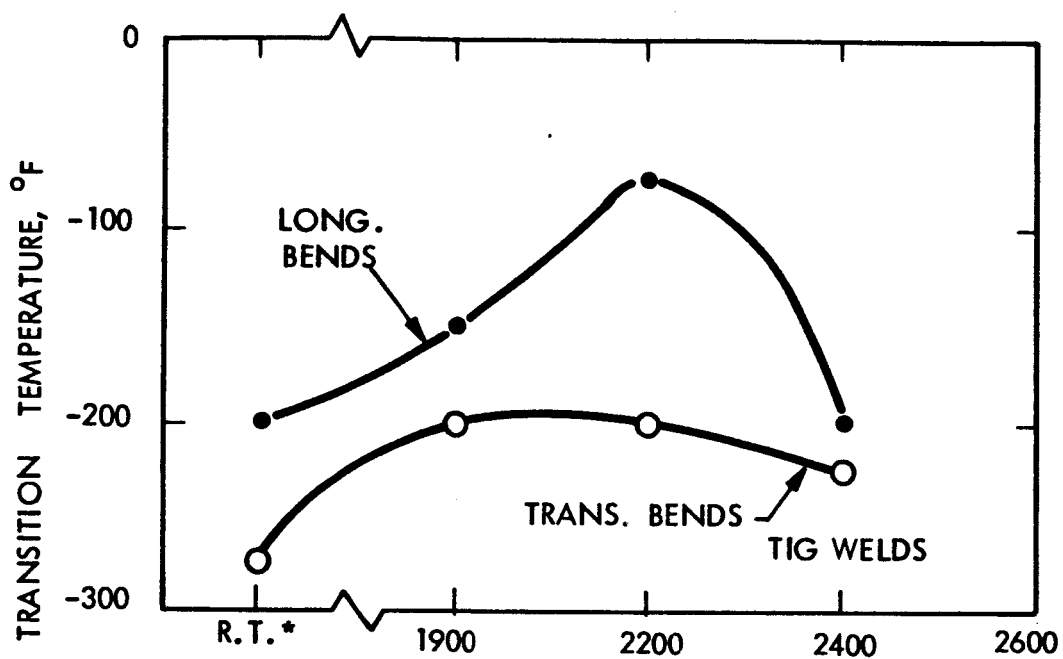
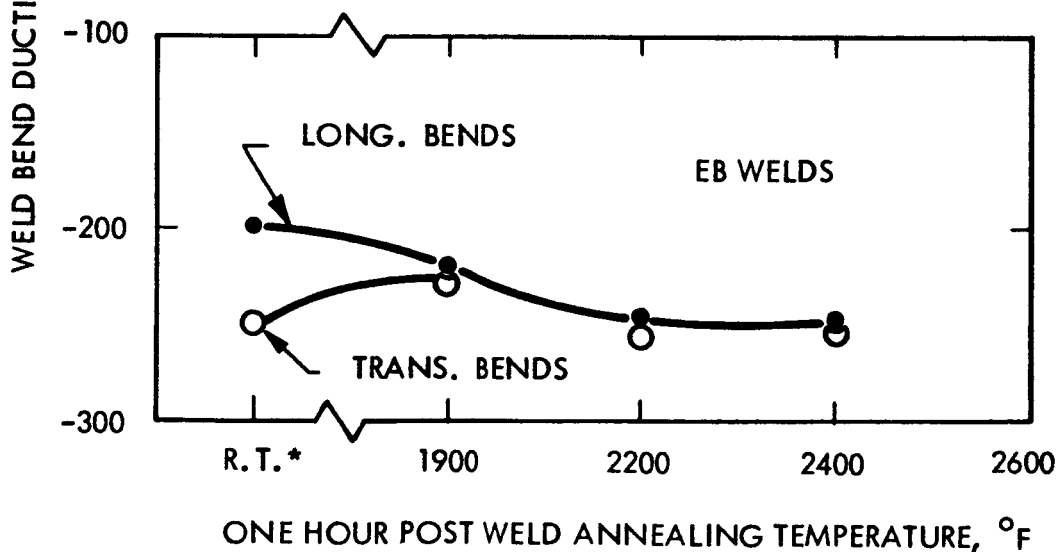


FIGURE 5 - Effect of Post Weld Annealing on B-66 Weld Ductility



\*AS WELDED



ONE HOUR POST WELD ANNEALING TEMPERATURE, °F  
605779B

FIGURE 6 - Effect of Post Weld Annealing on C-129Y Weld Ductility

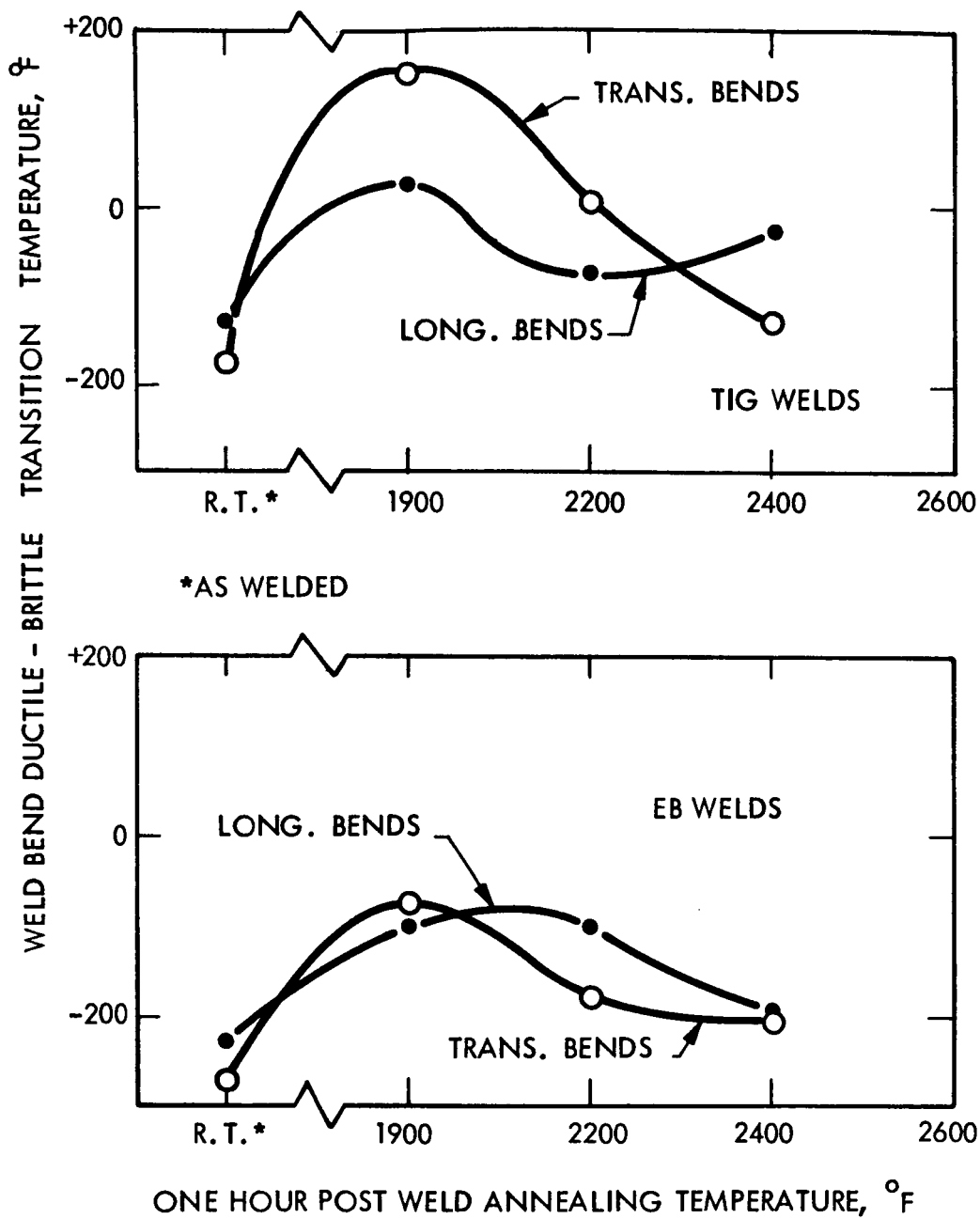
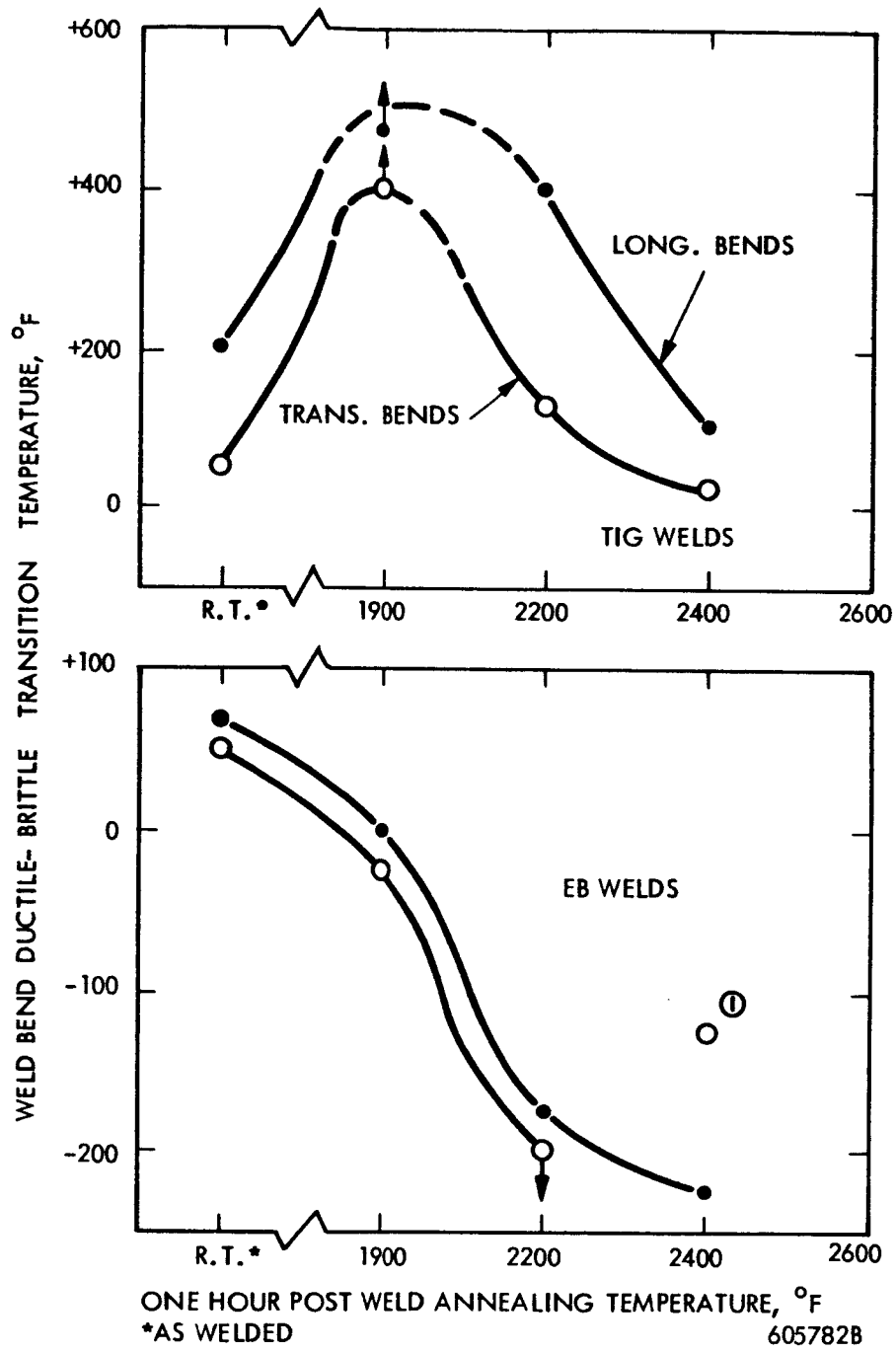


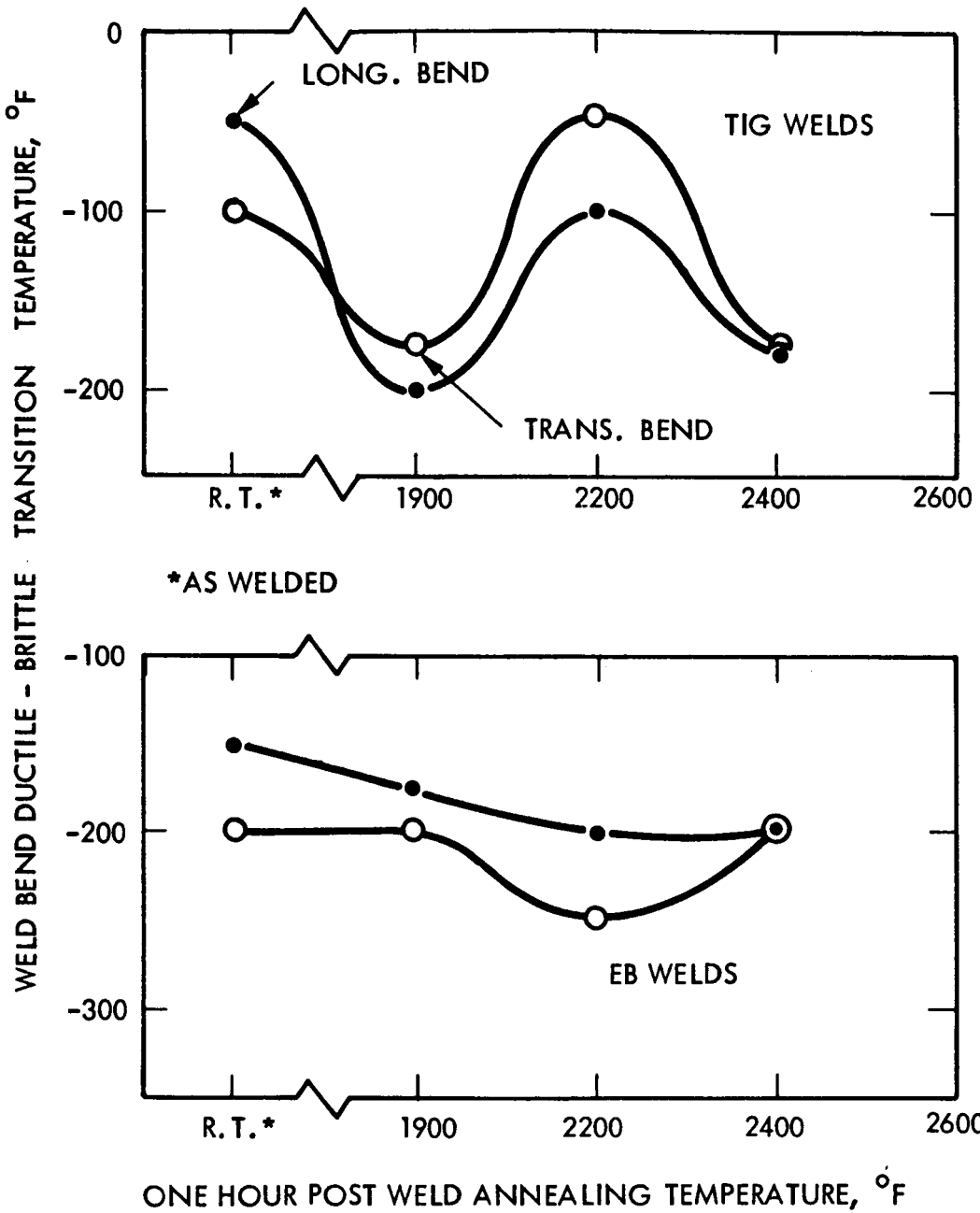
FIGURE 7 - Effect of Post Weld Annealing on Cb-752 Weld Ductility





① MAY APPEAR HIGH BECAUSE TRANSITION TEMPERATURE WAS NOT CLOSELY BRACKETED

FIGURE 8 - Effect of Post Weld Annealing on D-43 Weld Ductility



605783B

FIGURE 9 - Effect of Post Weld Annealing on FS-85 Weld Ductility

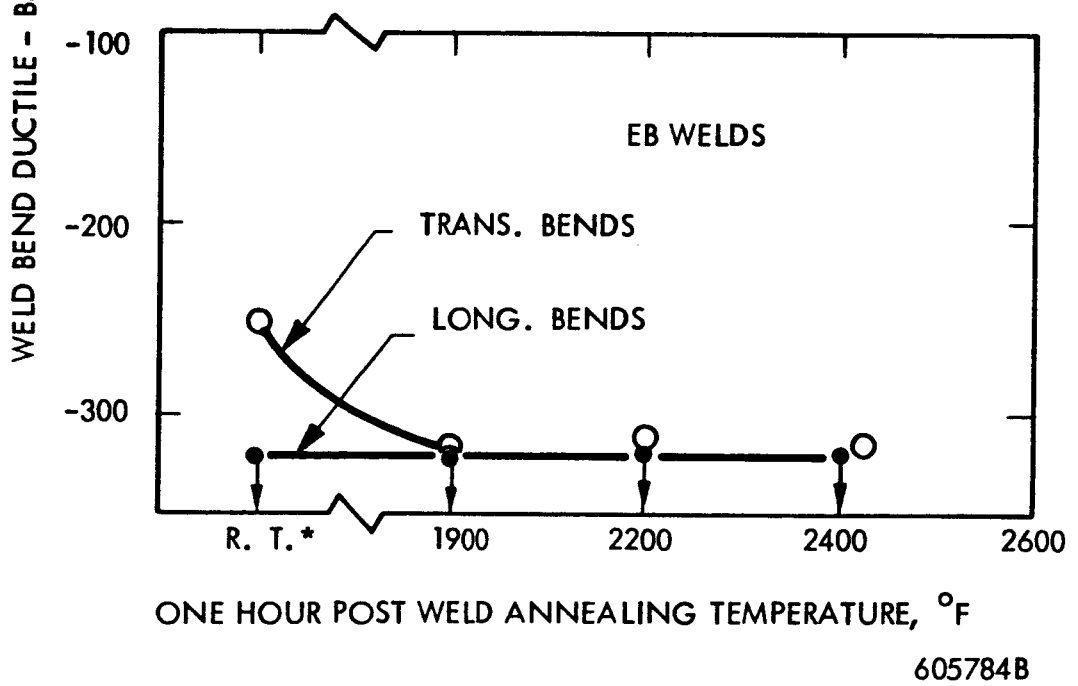
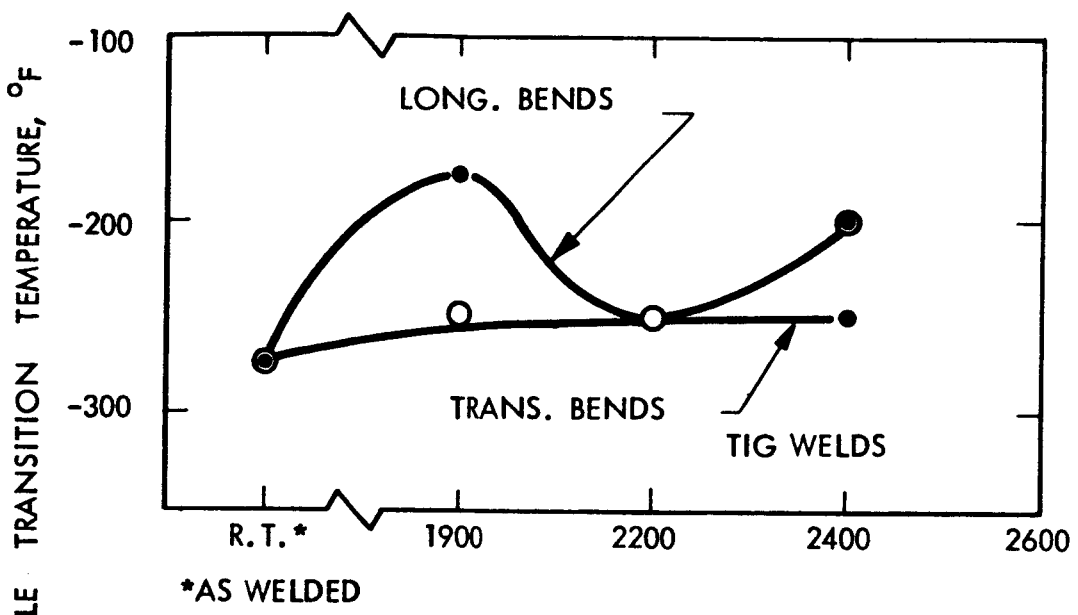
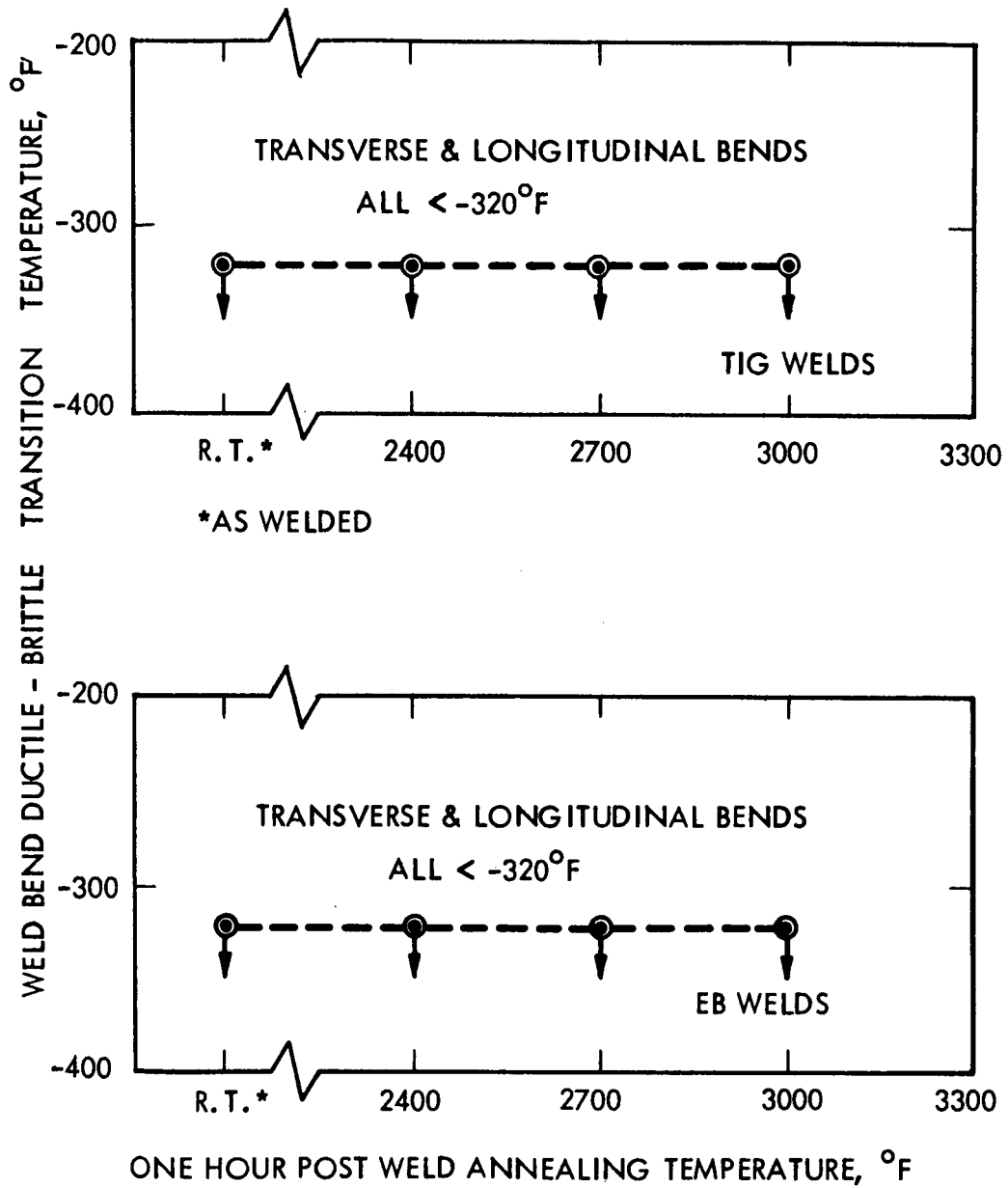
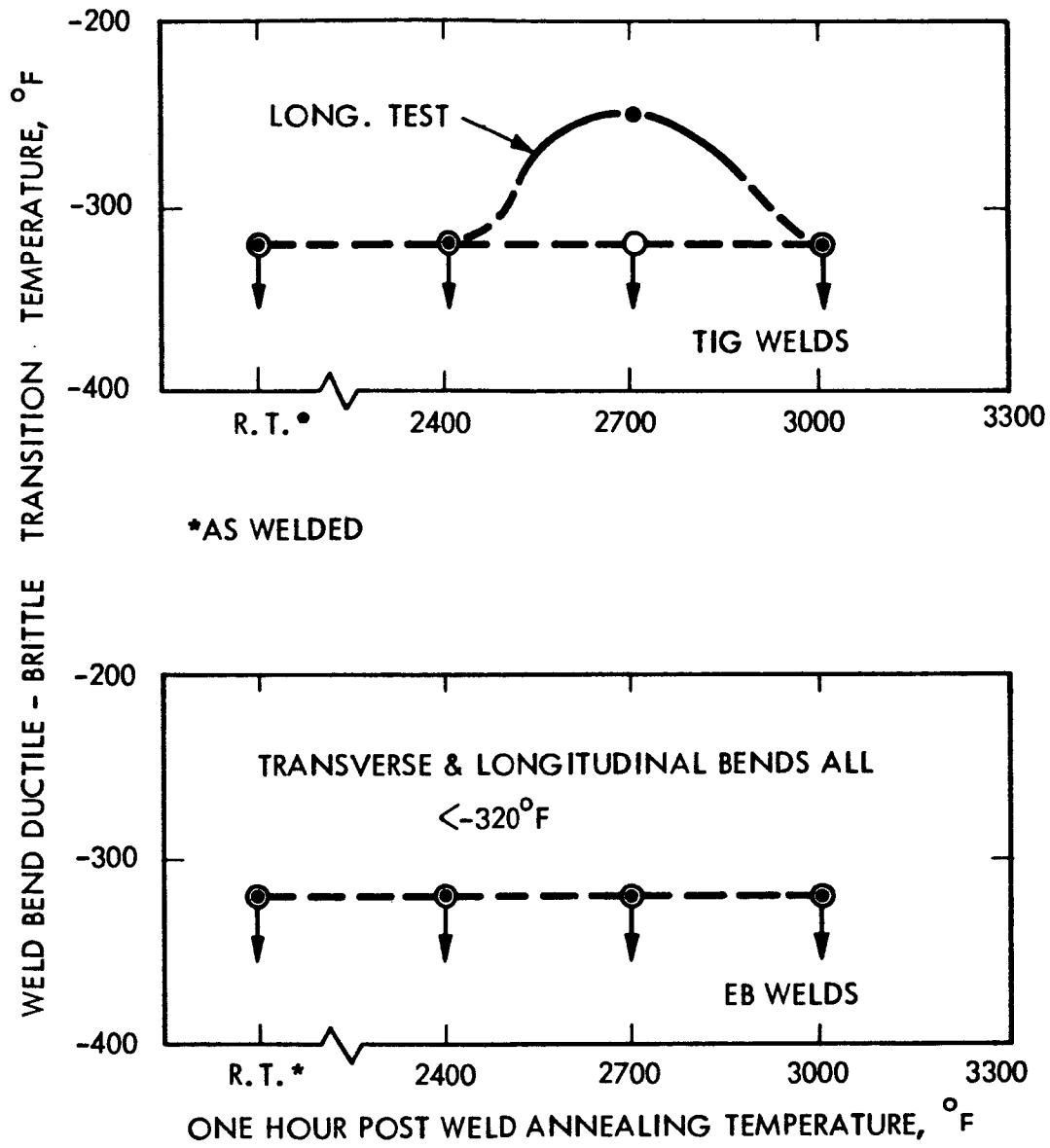


FIGURE 10 - Effect of Post Weld Annealing on SCb-291 Weld Ductility



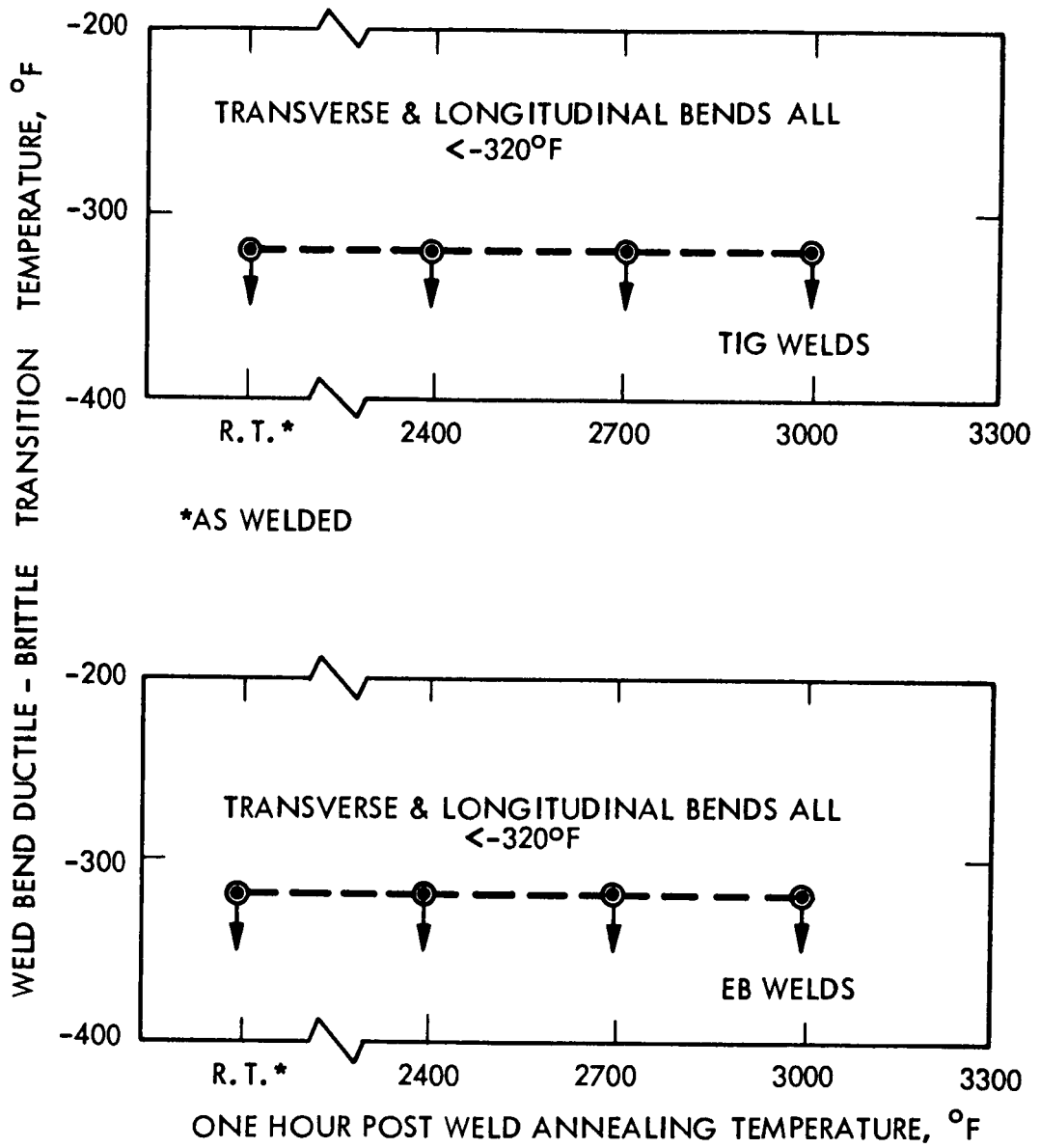
605785A

FIGURE 11 - Effect of Post Weld Annealing on T-111 Weld Ductility



605808B

FIGURE 12 - Effect of Post Weld Annealing on T-222 Weld Ductility



605776B

FIGURE 13 - Effect of Post Weld Annealing on Ta-10W Weld Ductility

Metallographic evaluation of the post weld anneal series of welds has been initiated.

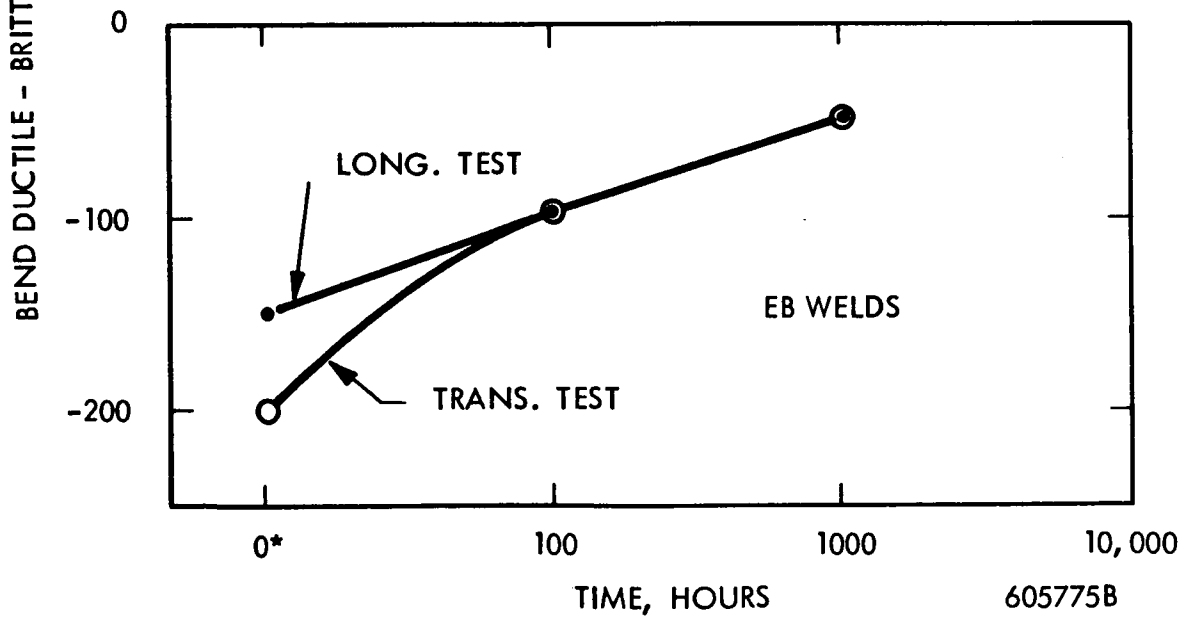
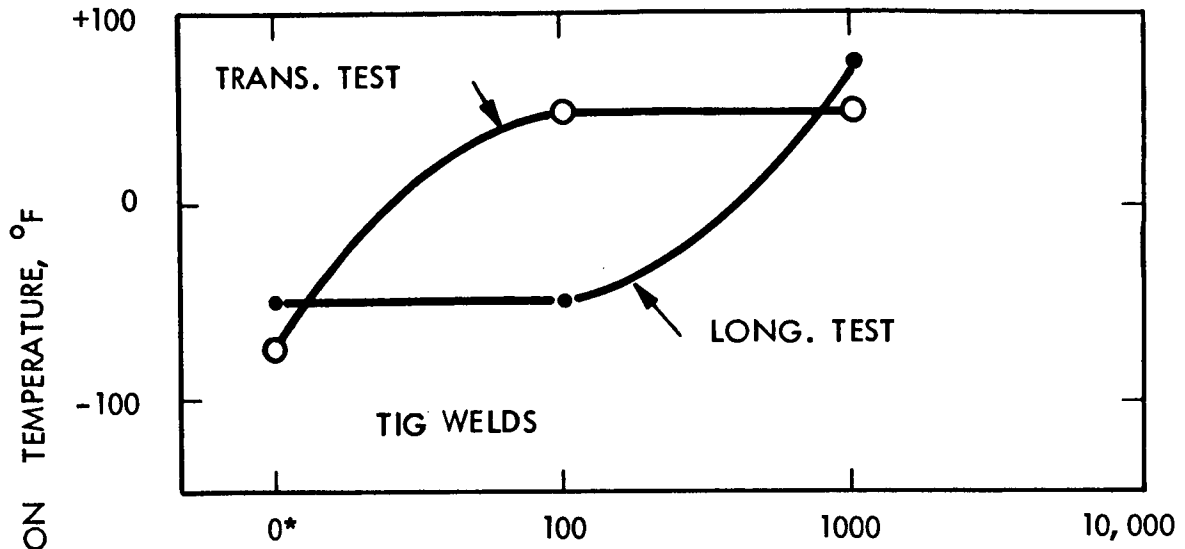
#### B. THERMAL STABILITY SCREEN OF FS-85, T-111, AND T-222

TIG and EB welds in 0.035 inch FS-85, T-111, and T-222 sheet were pre-screened for thermal stability. This was an additional effort, separate from the contemplated thermal stability studies, run specifically to obtain advance data on these alloys. Welds were annealed for 100 and 1000 hours at 1800°F in a  $10^{-10}$  torr vacuum to determine if they would respond to aging as measured by a shift in the bend ductile-to-brittle transition temperature. No post weld annealing was done prior to aging. Bend test results are summarized in Figures 14, 15, and 16. Hardness traverses were completed for the TIG welds. These are plotted in Figure 17.

All three alloys responded to aging with a measurable loss in ductility which may have been avoided by "overaging" prior to the 1000-hour test with a higher temperature post weld anneal. Differentiation of alloy behavior based on the relative transition temperature shift is difficult since both tantalum alloys had as-welded transition temperatures below -320°F, the lowest test temperature employed. Hence, as-welded transition temperatures were not known exactly for T-111 and T-222. Also, the degree of aging cannot be ascertained. T-222 welds appear to have been least affected by the 1800°F aging anneals.

FS-85 - Both TIG and EB welds in FS-85 showed about a 100°F increase in bend transition temperature after 1000 hours, Figure 14. Longitudinal and traverse bends displayed about equal aging responses. TIG and EB weld fractures were similar. Fractures originated in the weld, at the weld interface, or heat affected zone. The bend transition was abrupt, occurring generally within a 50°F range. Base metal resistance to fracture was not significantly better than weld metal resistance. Within 25°F of the DBTT, cracks in longitudinal test propagated entirely through the specimen without being arrested in the base metal.

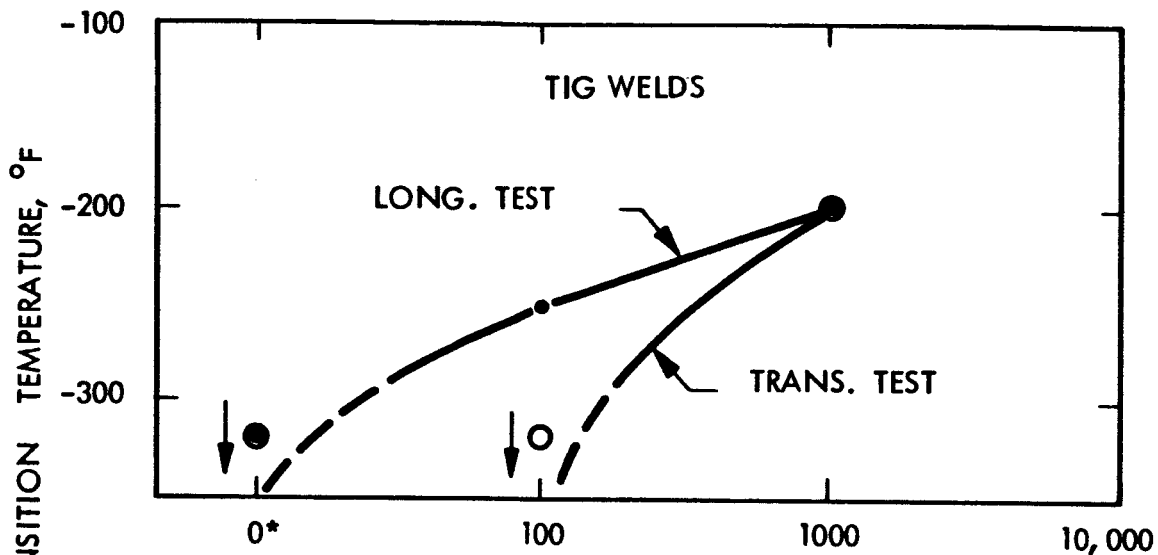
Metallographic examination of aged TIG welds revealed second phase precipitation accentuating ghost lines in the base metal and heat affected zone. Second phase precipitation also occurred in the solute rich weld areas, Figure 18. Similar second phase



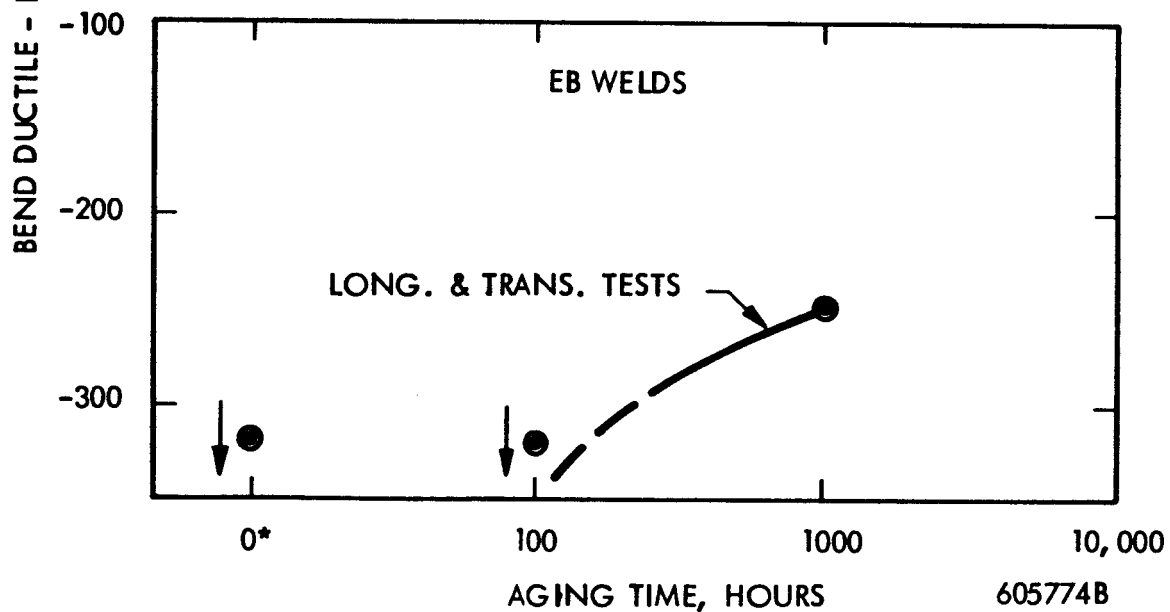
\*AS WELDED

FIGURE 14 - Effect of Aging at 1800°F on Welded FS-85





\*AS WELDED



605774B

FIGURE 15 - Effect of Aging at 1800°F on Welded T-111

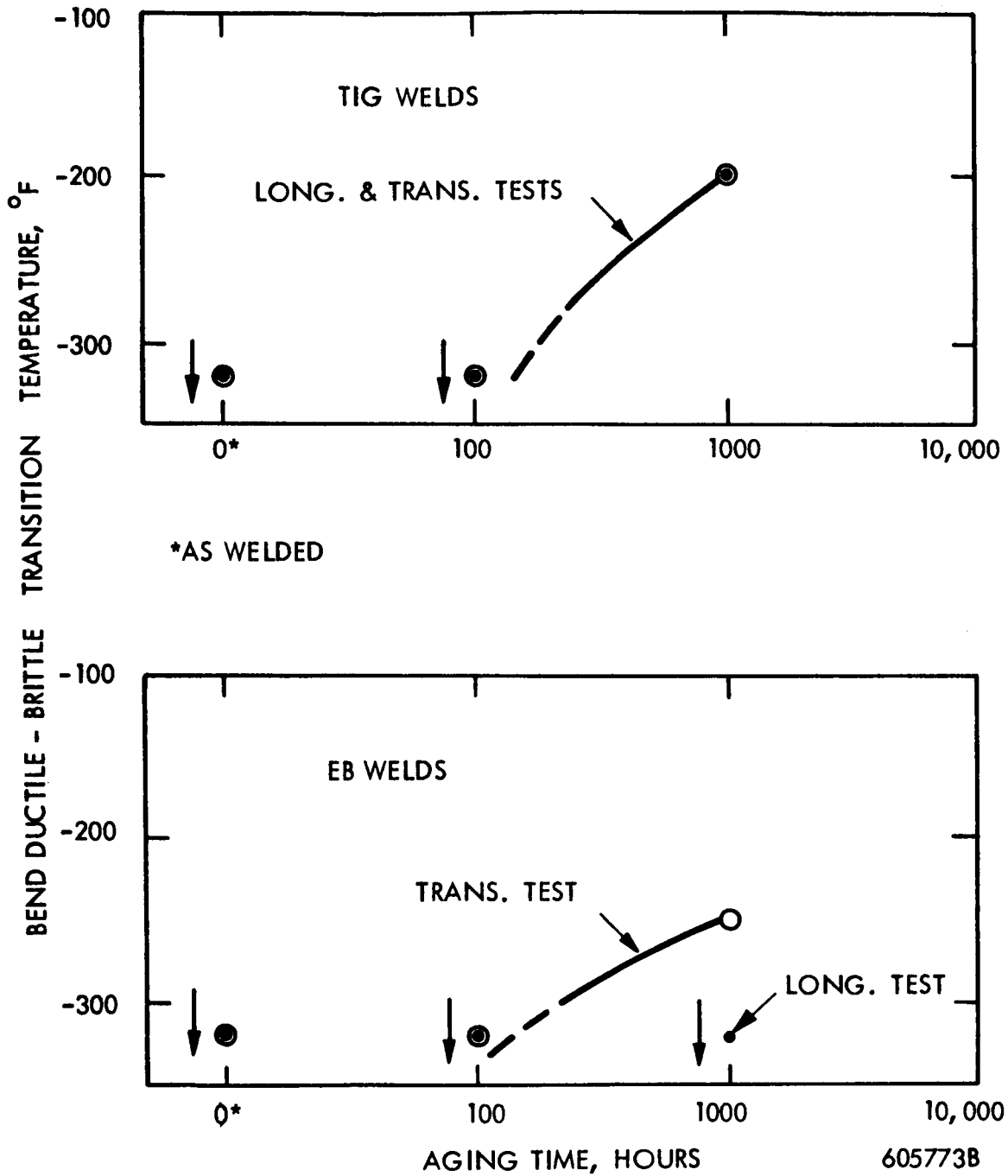


FIGURE 16 - Effect of Aging at 1800°F on Welded T-222

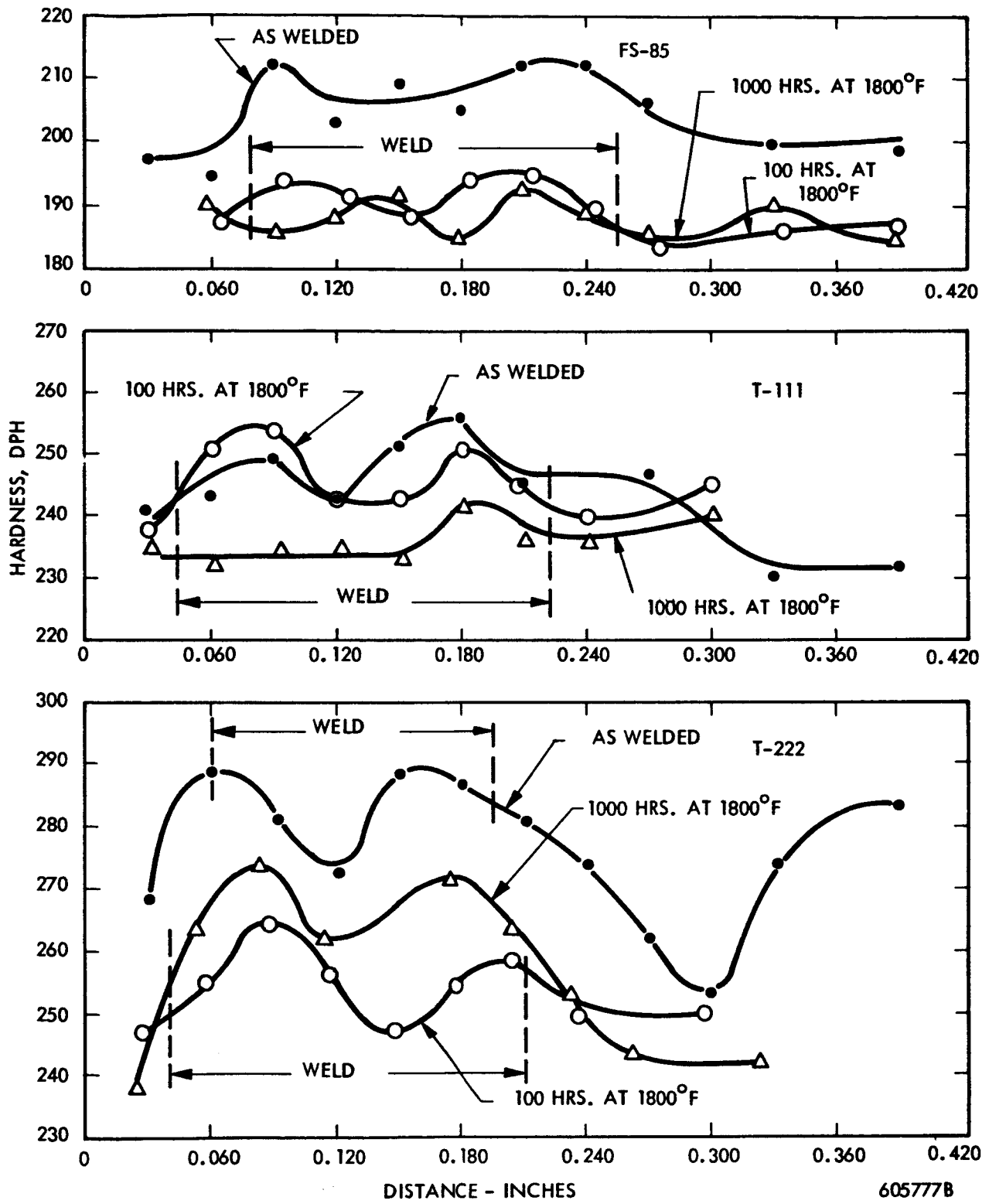


FIGURE 17 - Effect of Aging at 1800°F on FS-85, T-111 and T-222 TIG Welds



8670

200X



8990

200X

Base Metal



8670

200X



8990

200X

Weld Metal

As-Welded

Aged 1000 hrs at 1800°F

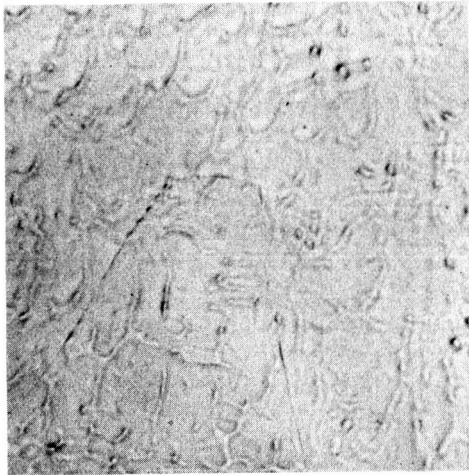
FIGURE 18 - Microstructure of FS-85 TIG Welds

precipitation has been noted elsewhere<sup>(2)</sup>. Hardness traverses, Figure 17, showed a general softening with aging which probably reflects the effect of stress relief and the loss of solid solution strengtheners through precipitation.

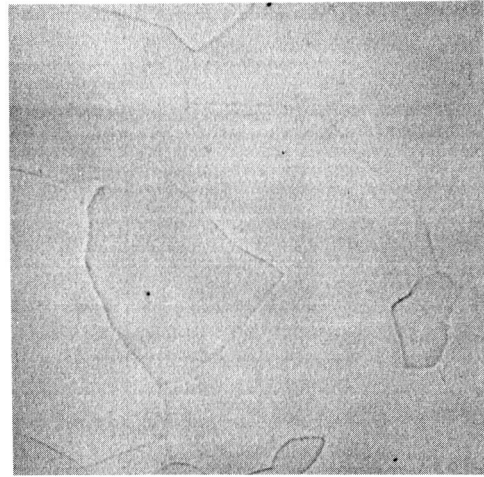
T-111 - Aging in T-111 TIG welds occurred within 100 hours, and in EB welds within 1000 hours. Fracture location and behavior indicated that loss of ductility with aging was restricted largely to the weld and was evidenced only as weld tears after considerable strain was observed (i.e. tearing occurred near the 90° target bend).

Metallography and hardness traverses of TIG welds in this system proved to be fairly interesting. The weld zone in T-111 (and T-222) had a slightly lower hardness in the center than at the edges, Figure 17. Metallographic examination revealed grains in which cellular growth occurred by two processes: epitaxial growth at the weld edges and nucleation and grain growth in the weld center. The epitaxial grains represent areas of slower grain growth and hence areas with a greater solute redistribution than would be expected in the area of nucleated grains where supercooling would result in high growth rates. This probably accounts for the hardness variation across the weld. The persistence of this effect through the 1000-hour age would result from a low solute (hafnium) diffusion rate at the 1800°F aging temperature.

Aged and as-welded microstructures of T-111 TIG welds are shown in Figures 19 and 20. Weld and heat affected zone matrices remained single phase but grain boundary precipitation occurred in both areas during aging, Figure 19. A peculiar base metal-heat affected zone interface reaction occurred, Figure 20. Careful examination revealed that the precipitate responsible for this situation could not be retained during polishing. Hence, the structures shown in Figure 20 are superficial to the extent that the apparent precipitates are actually precipitate locations which were attacked preferentially during etching. Heat affected zones of several aged welds were sheared out and dissolved using the bromine extraction technique. The extracted residue was identified by X-ray diffraction analysis. The primary precipitate was identified as defected hafnium monocarbide (Hf,Ta,W)  $C_{1-x}$ . Small quantities of  $Ta_2C$  and  $HfO_2$  were present. While T-111 is nominally a solid solution alloy, produced with no intentional carbon addition, the particular heat of T-111 obtained for this program has a carbon content of 50 ppm. Since the carbon solubility in T-111 at temperatures below 3000°F is very low, the existence of carbide precipitates in the

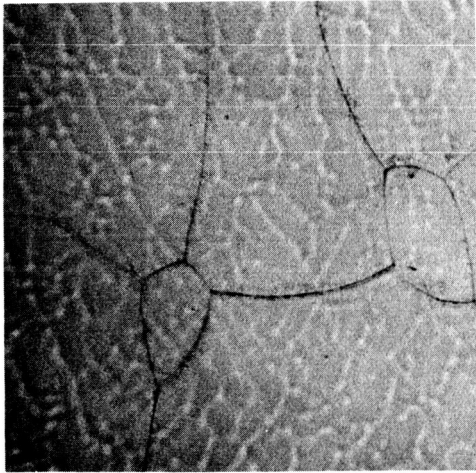


9663A Weld 500X

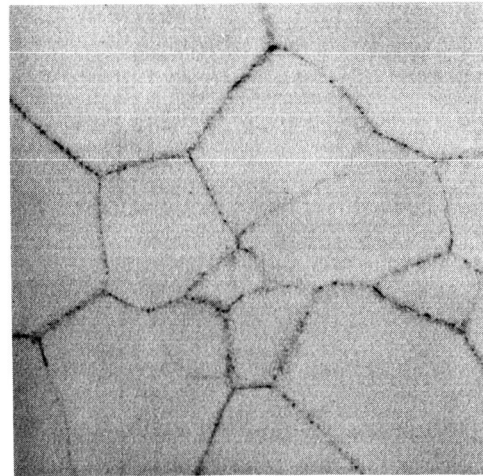


9663A HAZ 500X

As-Welded



9663 Weld 500X



9663 HAZ 500X

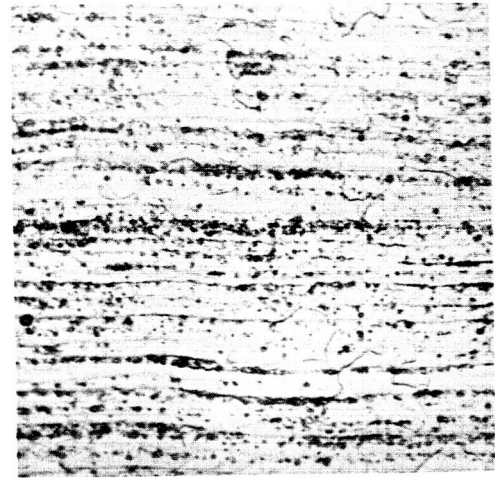
Welded and Aged 1000 Hours at 1800°F

FIGURE 19 - Weld and HAZ Microstructures of T-111 TIG Weld



9663A

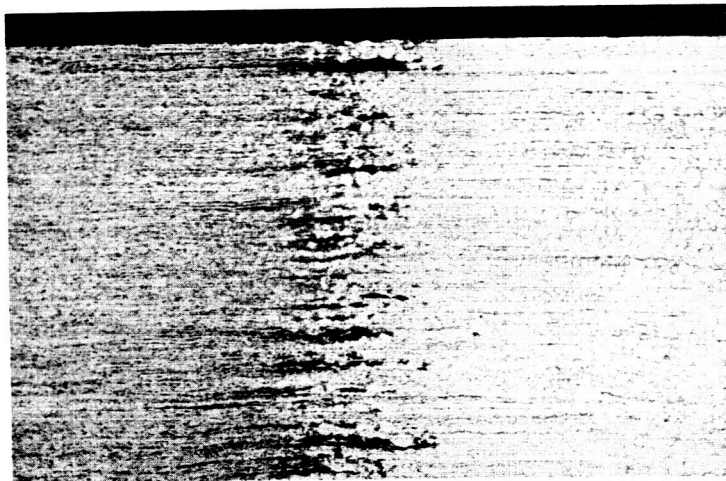
80X



9663A

500X

As-Welded



9663

80X



9663

500X

Welded and Aged 1000 Hours at 1800°F

FIGURE 20 - HAZ-Base Metal Area Microstructure of T-111 TIG Welds

microstructure is not unexpected. The phase relationships proposed by Ammon et al<sup>(3)</sup> for the tantalum rich corner of the Ta-W-Hf-C system indicate that both carbides could be observed in this alloy. The monocarbide would tend to occur in hafnium-rich areas which exist in the base metal<sup>(4)</sup> as well as the weld metal. This is verified by the preferential location of precipitates in Figures 19 and 20 at ghost structure flow lines in the base metal and grain boundaries in the weld and heat affected zone. The phase relationships also indicate that the final process annealing temperature used for T-111 (4 hrs at 2400°F) was marginal from the standpoint of homogenization even though adequate for recrystallization.

Hardness traverses correlated well with microstructural changes. General softening occurred in the weld zone which would be expected both because of stress relief and by grain boundary precipitation. Heat affected zone softening to base metal hardness levels also occurred through an apparent loss, by precipitation, of solid solution strengtheners. The initial as-welded heat affected zone hardness must result from the solid solutioning effect of the weld thermal cycle. Hardening occurred with aging in the heavily precipitated area of the heat affected zone-base metal interface.

T-222 - Aging in T-222 TIG and EB welds occurred after 1000 hours as indicated by a shift in the bend transition temperature, Figure 16. Fractures were restricted principally to the weld and frequently propagated along the weld centerline. Weld hardness traverses, which indicate an overage after 100 hours and secondary aging after 1000 hours, tend to confirm the bend test response. Based on the hardness traverses, the as-welded heat affected zone exhibits a combination of overaging and solution anneal strengthening. Further overaging of the heat affected zone occurred during the annealing treatment.

TIG weld metallography displayed a fairly clean microstructure throughout the weld and base metal. Some grain boundary precipitate in the weld and heat affected zone was noted after aging. The base metal-heat affected zone precipitate observed in T-111 welds was absent in the T-222 welds. Since similar base metal reactions would be expected in these alloys, the absence of this precipitate zone in T-222 probably results from the difference in final anneals for the two alloys during processing of the sheet by the supplier; one hour at 3000°F for T-222 and four hours at 2400°F for T-111. The fact that the T-111 heat



affected zone was clean after aging indicates that a higher temperature final recrystallizing (also solutioning) anneal would have stabilized this alloy with respect to the heat affected zone-base metal interface reaction.

Metal Vapor Mass Transfer - Welded specimens of three refractory metal alloys, T-111, T-222, and FS-85, were randomly stacked and wrapped in tantalum foil for 1800°F, 100 hour and 1000 hour aging runs. Following the 100 hour age, the inside of the foil and the specimen surfaces were observed to be stained. The discoloration, mostly dark blue, was quite disturbing since this is characteristic of contamination. However, x-ray fluorescence analysis showed that the stained side of the foil contained a high concentration of hafnium and a trace of zirconium compared to the clear outside surface of the foil which had neither element present. Apparently, hafnium from T-111 (Ta-8W-2Hf) and T-222 (Ta-9.6W-a.4Hf-0.01C) and zirconium from FS-85 (Cb-27Ta-10W-1Zr) were evaporating from the specimens and condensing on the foil as thin films causing interference surface discoloration. The specimens were also stained in the same manner but these were unpacked without noting their relative positions so that adjacent specimen effects could not be correlated.

The 1000 hour age offered a second opportunity to observe this phenomenon. Specimen orientation was carefully noted when unwrapping these specimens and a consistent story developed. Adjacent specimens, similar or dissimilar, shadowed one another. Shadows were thrown by the base metal and preferentially adsorbed by the weld and heat affected zone of the adjacent specimen. Vapor transfer is the apparent mechanism involved, while concentration differences at the surfaces of adjacent specimens generate the driving force for the constituent transfer. Coring in the weld and incipient melting in the heat affected zone followed by pickling prior to annealing would result in a depletion of hafnium or zirconium near the surface in these areas and account for their being preferentially shadowed by adjacent specimens and also their failing to throw shadows on adjacent specimens.

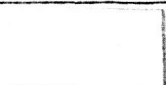
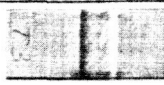

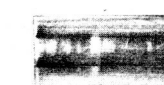
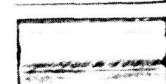







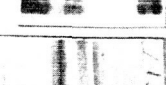

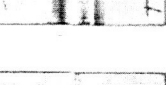




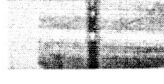


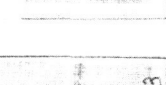


One group of specimens which were annealed at 1800°F for 1000 hours is shown in Figure 21. There were two stacks of specimens in this package as indicated in this figure. Specimens were examined and laid down in sequence as they were unpacked and photographed.

This figure demonstrates the effect fairly clearly even though it is slightly flat due to the photographic difficulty resulting from lighting back reflection. Also, note that only one side of each specimen is shown whereas the comments in some cases apply to the backsides of the specimens. Arrows placed next to a specimen indicate that it shadowed the facing specimen. Several specimens show this effect clearly. The T1 TIG weld, second from the top of Stack No. 2, was shadowed by the T1 EB weld, third from the top. The TIG weld and its heat affected zone were shadowed opposite the EB weld base metal but not opposite the EB weld proper (clean area across TIG weld). In Stack No. 1 the C3 TIG weld, sixth weld down, was obviously shadowed by the T1 TIG weld, seventh down, except at the facing area directly opposite the weld. Again the shadowed specimen was most affected in the weld and heat affected zone area.

In Figures 21 and 22, specimens marked T1, T3, and C3 are alloys T-111, T-222, and FS-85 respectively. Interestingly, specimens annealed at 2400°F have been clean and free of discoloration. Apparently, diffusion of the vapor deposited film into the base metal occurs much more rapidly at 2400°F.

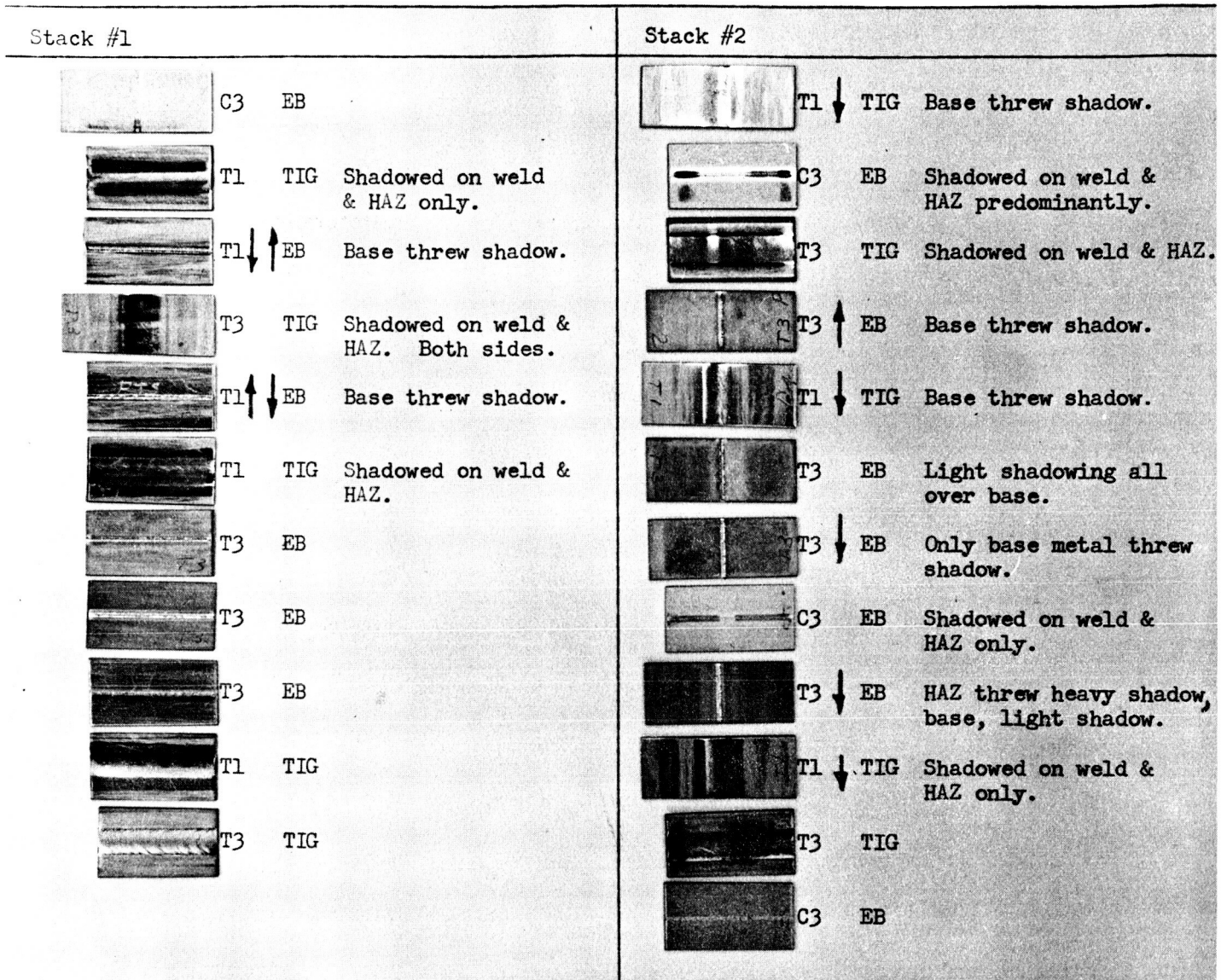
### C. EFFECT OF OXYGEN CONTAMINATION ON THE WELDABILITY OF REFRACTORY METAL ALLOYS

Additional work has been initiated to evaluate the effect of oxygen contamination on the weldability and thermal stability of selected refractory metal alloys. This program is designed to help fill an important technology gap, namely, the comparative effect of low level oxygen contamination on several promising refractory metal alloys. This is important in the selection of alloys for vacuum application since even the best high vacuum environment is a source of contamination capable of degrading alloy properties. For any one alloy the extent of damage occurring is a function of both the rate of reaction with the environment and the sensitivity of the alloy to the contaminant. An important measure of material degradation is change in weldability which, in refractory metal alloys, is a sensitive and realistic measure of the response to increasing contamination. Obviously, retention of good weldability with increasing low level contamination is a desirable alloy characteristic particularly since it is doubtful that complex long life systems would be operated without intermittent modification.

Stack #1		Stack #2	
	C3 TIG		T3 TIG
	C3 EB		T1 TIG Shadowed on weld & HAZ.
	T3 TIG Base & HAZ shadowed.		T1 ↑ EB Base threw shadow.
	C3 TIG Weld & HAZ shadowed.		T1 ↓ EB Base threw shadow.
	C3 ↑ ↓ EB Base threw shadow.		C3 TIG Weld & HAZ heavily shadowed, base lightly.
	C3 TIG Weld & HAZ shadowed.		T3 ↓ TIG Base threw shadow.
	T1 ↑ TIG Weld & HAZ shadowed. Base threw shadow.		C3 TIG HAZ shadowed by T3 above. Weld & HAZ heavily shadowed, base lightly.
	T1 ↑ ↓ EB Base threw shadow		T1 ↑ ↓ EB Base threw shadow
	C3 ↓ TIG Weld & HAZ shadowed.		C3 EB Weld & HAZ heavily shadowed, base lightly.
	C3 ↑ TIG Weld & HAZ shadowed. Base threw shadow.		C3 TIG Shadowed on weld & HAZ.
	C3 ↑ EB Base threw shadow. Weld, HAZ, base shadowed.		T3 ↑ EB Base threw shadow.
	T1 ↑ EB Base threw shadow.		T3 TIG
	T1 EB		

473-1

FIGURE 21 - Vapor Deposit Shadowing Effect Observed on Adjacent Specimens Annealed 1000 Hours at 1800°F. Arrows Indicate Specimen From Which, and Specimen Onto Which Shadows Were Thrown.



473-2

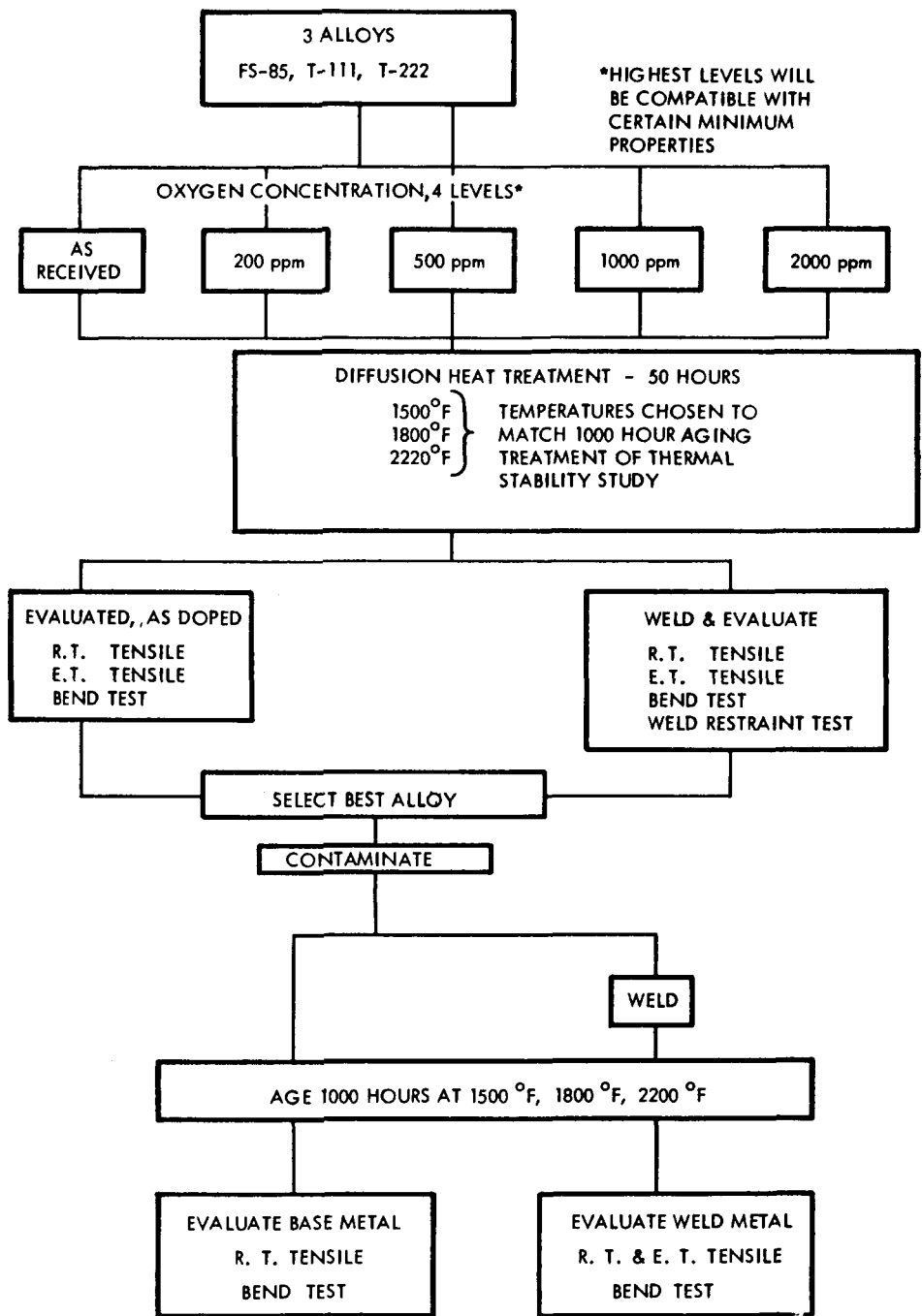
FIGURE 22 - Vapor Deposit Shadowing Effect Observed on Adjacent Specimens Annealed 1000 Hours at 1800°F. Arrows Indicate Specimen From Which, and Specimen Onto Which Shadows Were Thrown

Three alloys have been selected for this evaluation: FS-85 (Cb-27Ta-10W-1Zr), T-111 (Ta-8W-2Hf), and T-222 (Ta-9.6W-2.4Hf-0.01C). Each alloy will be tested in the as-received condition (also as-welded) and then contaminated at four levels and evaluated again by welding and testing. The oxygen contamination levels will span the range from the as-received material to the point of obvious ductility impairment. The testing program outlined will provide a measure of weld hot tear sensitivity, base and weld metal ductile-to-brittle transition temperatures, room temperature and elevated temperature tensile properties, weld quality (non-destructive testing), structural changes, and chemistry changes.

Gas-oxidation is being used, followed by a vacuum heat treatment to provide a minimum oxygen concentration gradient through the material thickness. Figure 23 outlines the overall program which includes a 1000 hour thermal stability evaluation for the most promising alloy.

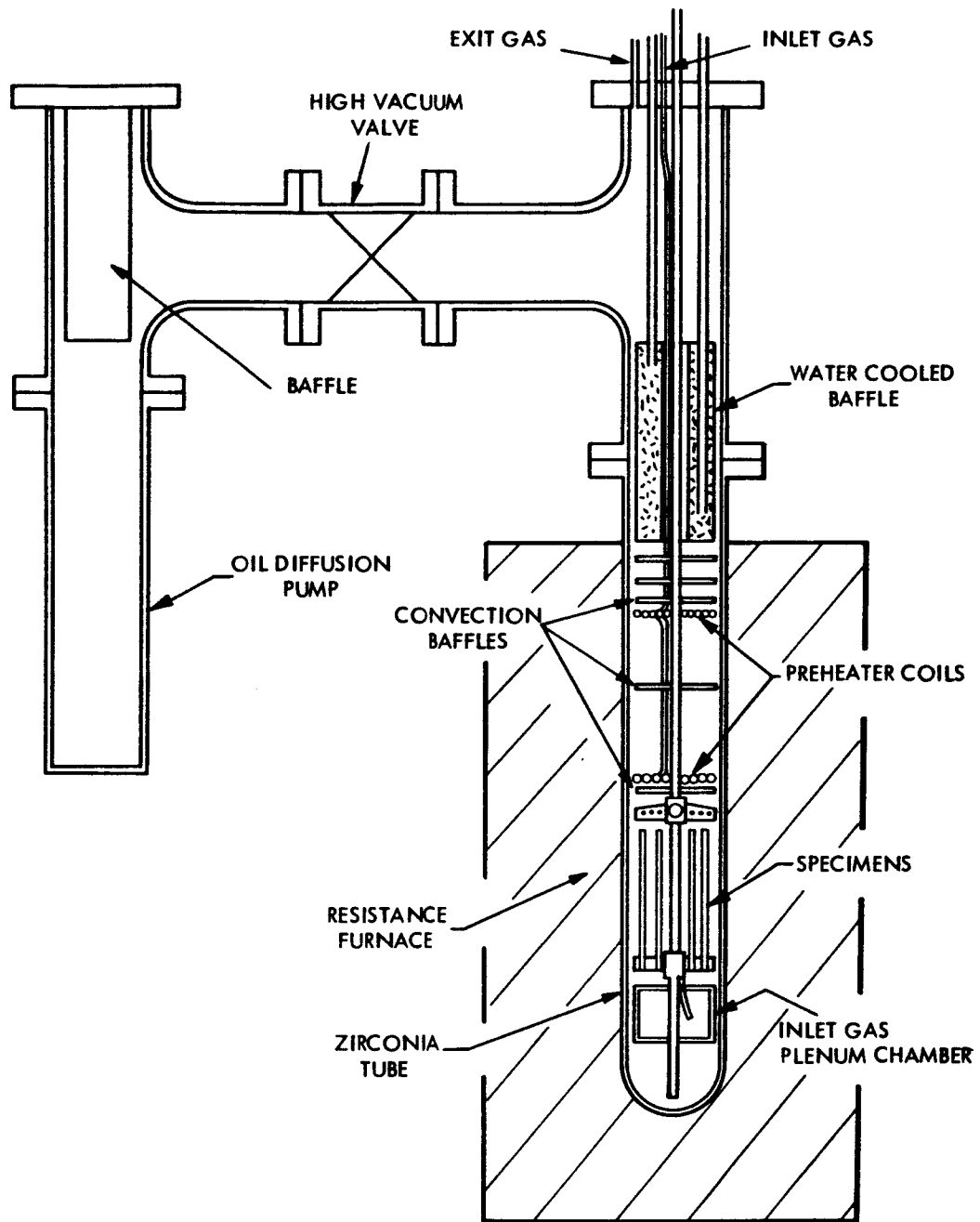
Helium carrier gas doped with 100 ppm of oxygen was selected as a contamination medium to provide more uniform oxidation of large samples than could be expected using other gaseous oxidation or anodization methods. Since one of the evaluation temperatures for the 1000-hour age and tensile testing is to be 1500°F (the other temperatures are 1800°F and 2200°F), 1500°F was the maximum doping temperature that could be used to avoid exceeding subsequent testing temperatures. For this reason initial contamination temperatures investigated were at or below 1500°F. Higher doping temperatures would be expected to provide higher diffusion rates and correspondingly more uniform contamination over the material cross section. A background of data on the low partial pressure oxidation rates of columbium and tantalum was available indicating reasonable reaction rates would occur at 1500°F. <sup>(5,6,7,8,9)</sup>

The retort assembly shown schematically in Figure 24 was designed to provide a uniform temperature reaction chamber capable of being vacuum purged and baked out at  $10^{-6}$  torr prior to the oxidation run. The assembly is made from type 304 stainless steel which forms a protective oxide layer at lower oxidation temperatures. A preheater arrangement is used for the incoming oxygen doped helium to permit high gas flow rates without perturbing the furnace temperature distribution. Figure 25 is a photograph of the retort assembly and Figure 26 shows the gas supply and monitoring system servicing the reaction chamber.



605807A

FIGURE 23 - Program Outline for Contaminated Alloy Weldability Evaluation



605772B

FIGURE 24 - Schematic of Oxygen Doping Apparatus

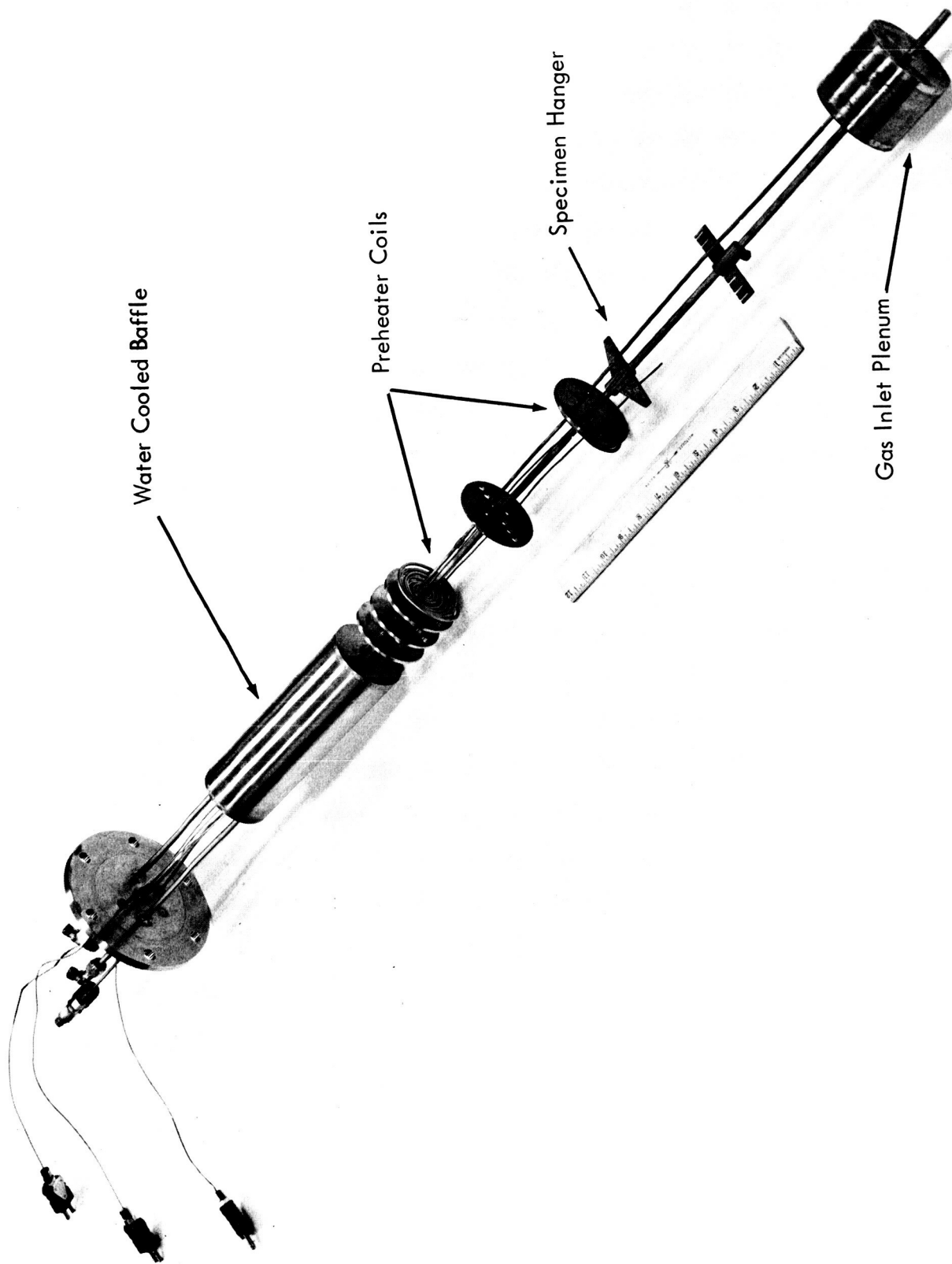


FIGURE 25 - Oxygen Doping Furnace Fixture



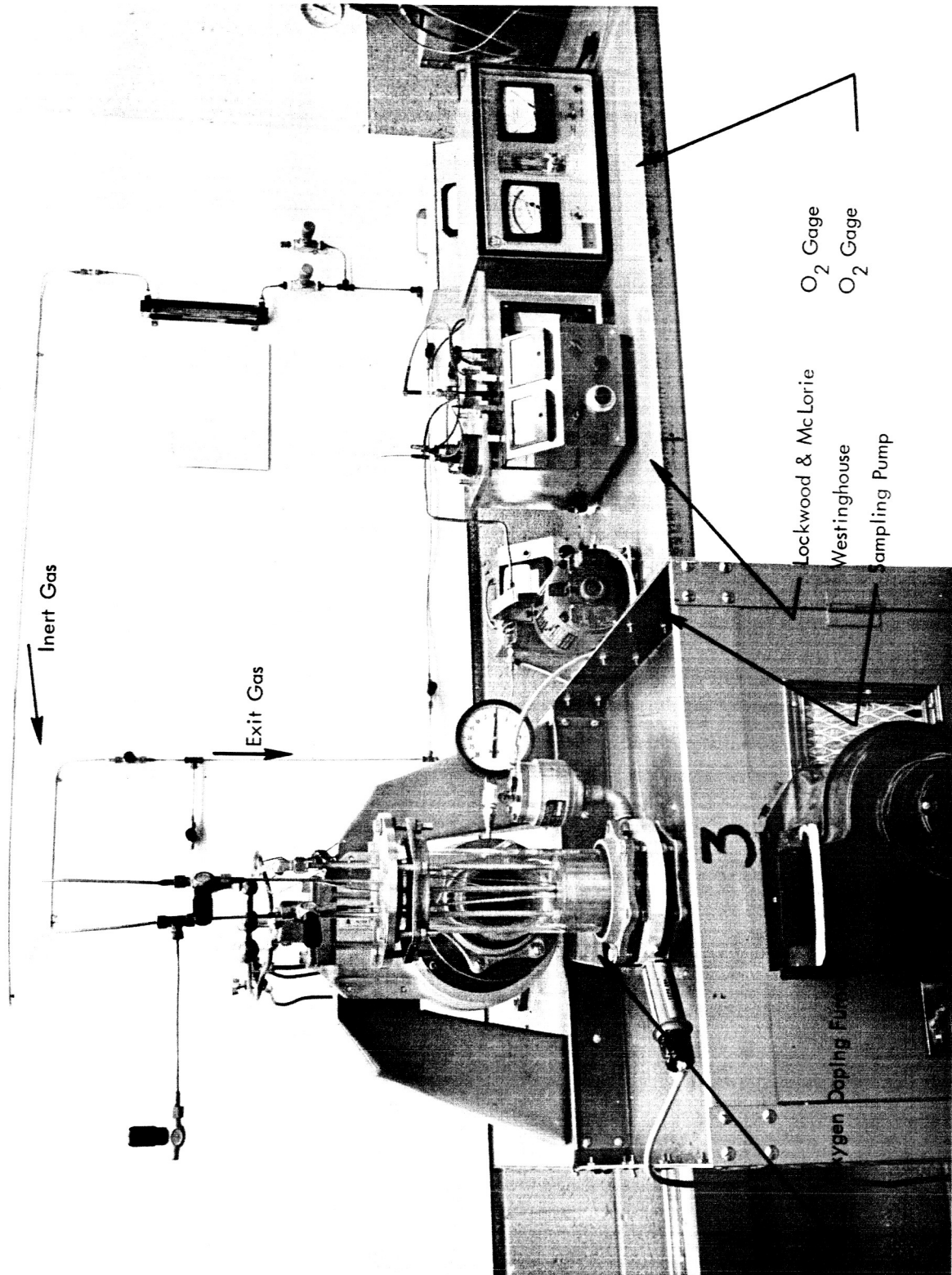
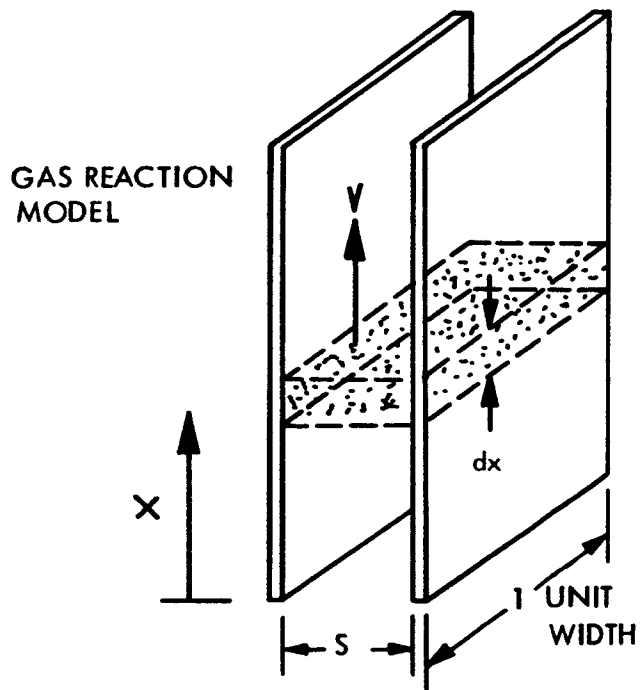


FIGURE 26 - Oxygen Doping Furnace and Gas Handling Equipment

The monitoring system allows both the inlet and outlet gas to be monitored for oxygen content as a check on the reaction rate and system leak tightness.

Initial reaction rates measured at 1500°F (815°C) were higher than expected to the extent that even a small furnace load would consume oxygen faster than it could be supplied by the carrier gas. Also, the reaction rate was noted to be strongly dependent on oxygen partial pressure, giving rise to a non-uniform oxidation condition. This is demonstrated in the relationship shown in Figure 27 wherein an expression was developed relating gas flow rate, reaction rate, and specimen spacing to oxygen depletion in the contaminating gas stream as the gas flows along the specimen surface. Specimen contamination would vary linearly with the oxygen partial pressure in the doping gas. Hence, for the high reaction rates observed at 1500°F, high contamination levels would occur at the specimen bottom and low levels at the top. Figure 28 is a curve developed from the oxygen depletion expression relating the process correction required in terms of reaction rate, gas flow rate, channel spacing and/or specimen geometry to avoid appreciable oxygen depletion in the carrier gas. From Figure 28, limiting the oxygen depletion in the exit gas to 10% (90% of inlet) would require a process correction factor of about 2000. This process correction could be achieved by reducing the reaction rate by 100 and increasing the gas flow rate by a factor of 20 without changing the load size or geometry.

In an attempt to reduce the reaction rate, lower temperatures from 750°F to 850°F, were investigated with two fold results. The reaction rate had decreased appreciably, by a factor of 40, and an analysis of contamination rates at different oxygen partial pressures indicated a negligible oxygen partial pressure dependence. Encouraging results with FS-85, which formed a visually uniform adherent black oxide film at 800°F led to a trial with full size sheet specimens. Figure 29 is a photograph of FS-85 oxidized to 700 ppm O<sub>2</sub>. The black oxide film is subsequently diffused into the sample by a 10<sup>-8</sup> torr vacuum heat treatment at temperatures of 1500°F, 1800°F, or 2200°F. Weight change measurements have proven to be adequate for in-process oxygen pick-up determinations. Initial chemical analyses have indicated no nitrogen or carbon pick-up either in the columbium or tantalum alloys. Bead-on-plate welds have been made on process evaluation samples and both base



FIND  $C$  ( $O_2$  CONCENTRATION  
IN HELIUM IN g/cc)

AS A FUNCTION OF  
DISTANCE ALONG  
CHANNEL

$C_o$  = INITIAL CONCENTRATION

REACTION RATE IS PROPORTIONAL  
TO  $O_2$  CONCENTRATION

$$R = kC$$

$$V = \text{cm/sec}$$

$$dx = vdt$$

MASS FLOW RELATION

$$Q = (\text{gm}O_2)$$

1.  $Q \text{ IN} = Q \text{ OUT} + Q \text{ REACTED}$
2.  $Q \text{ OUT} = Q \text{ IN} - Q \text{ REACTED}$
3.  $C_f(X) = C_o e^{-\frac{2kx}{Sv}}$

605806A

FIGURE 27 - Relationship of Doping Variables and Depletion of Oxygen  
in the Helium Carrier Gas.

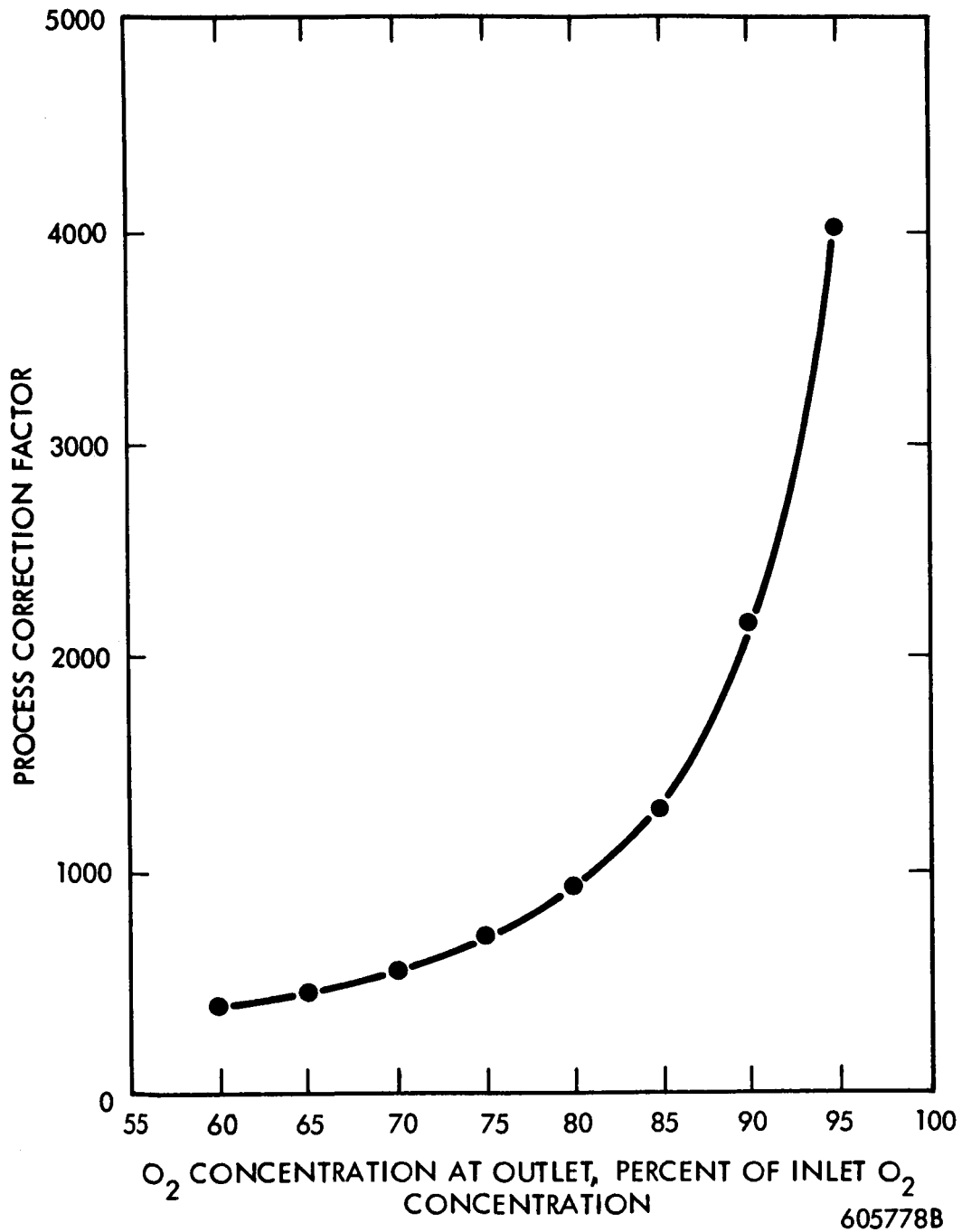


FIGURE 28 - Process Correction Curve Based on Observed 1500°F Oxidation Rate (Using 100 ppm Oxygen Doped Helium at 100 cc/min Flow Rate)

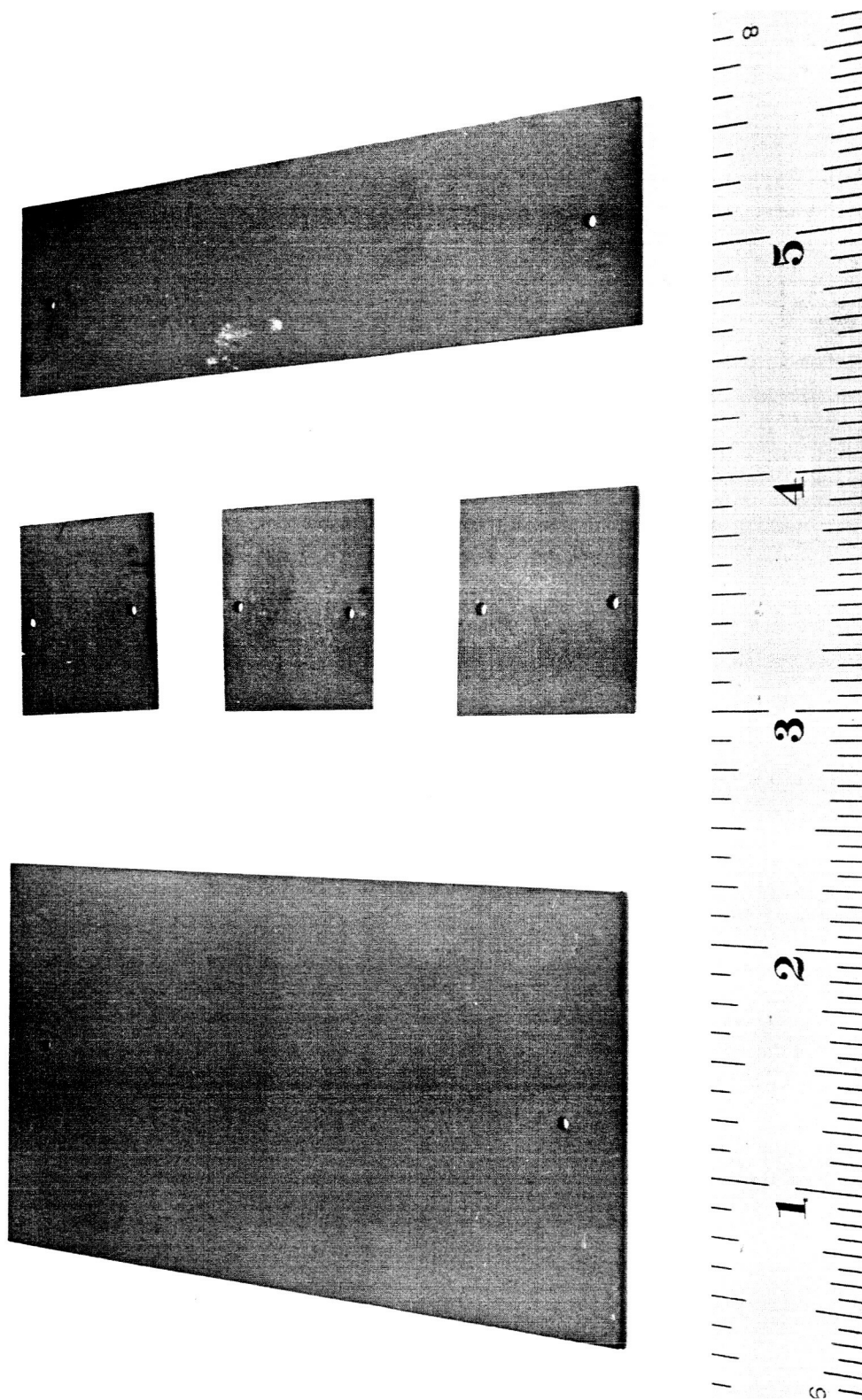


FIGURE 29 - FS-85 Doped to 750 ppm Oxygen (Prior to Diffusion Heat Treatment)

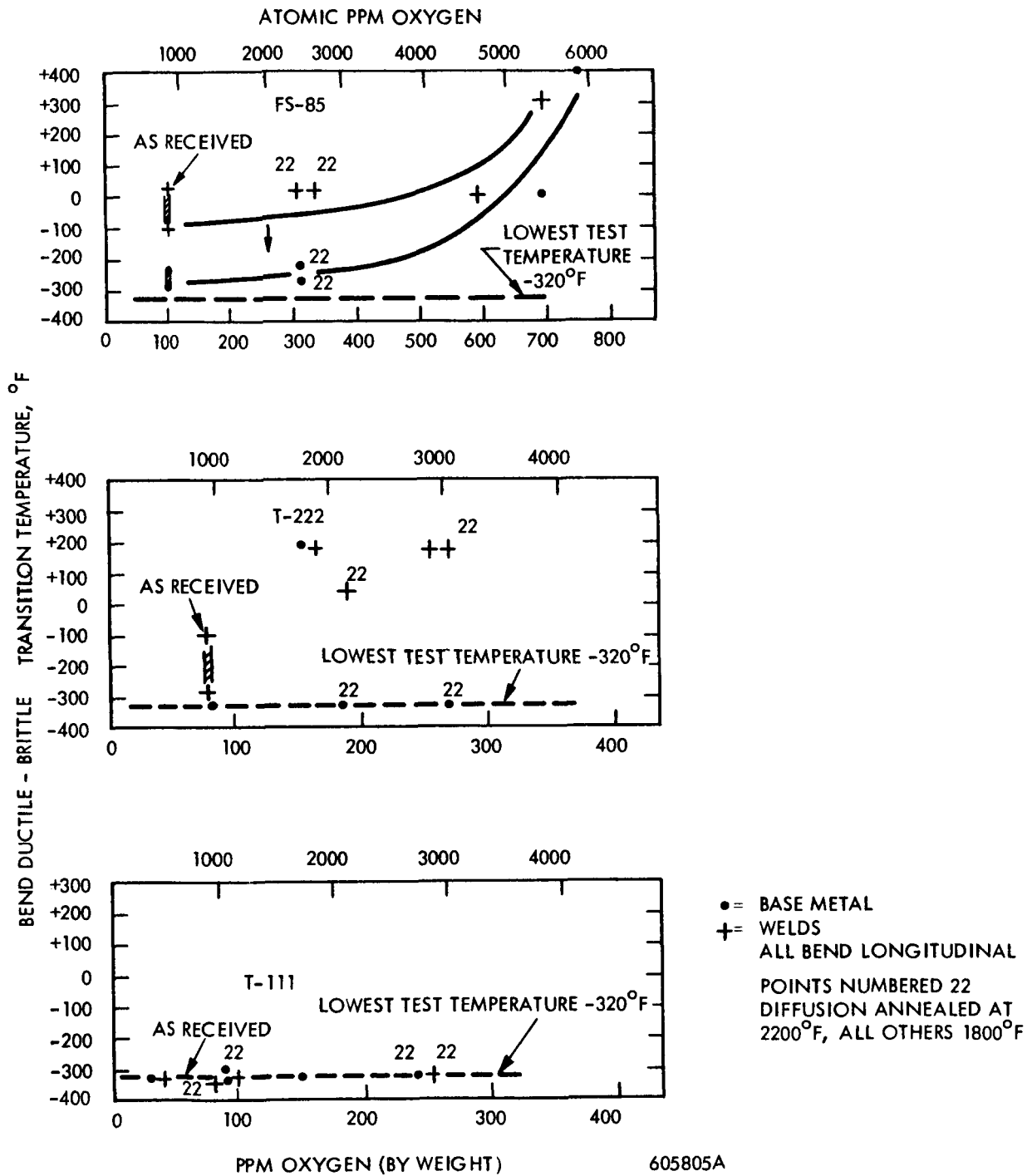


FIGURE 30 - Bend Ductility as a Function of Oxygen Content

and weld metal bend ductility tests have been run on contaminated FS-85, T-111, and T-222. The results appear to discriminate substantially between the ductility of T-111 and T-222 at the 150-200 ppm O<sub>2</sub> level. Figure 30 compares the bend ductility of the three alloys as a function of the oxygen content. FS-85 appears to be tolerant of oxygen additions up to 400 ppm. T-222 begins to show a loss of bend ductility at 150 ppm oxygen in both the base and weld metal following diffusion treatments at 1800°F or below. The 2200°F diffusion treatment restores the base metal bend ductility to -320°F, although the weld metal ductility is unaffected indicating that the higher temperature diffusion treatment produced a more favorable distribution or form of oxide in the base metal. The welding operation produces a complete oxygen redistribution in any case and, as expected, weld ductility was unaffected by the prior diffusion treatment. Bend tests made on T-222 diffusion treated at 1800°F and below have produced multiple ragged tears indicative of poor surface ductility which correlates with the high surface hardness noted in microhardness traverses. T-111 base and weld metal has produced ductile bends at -320°F for oxygen concentration levels up to 200 ppm.

This data is only preliminary and following the completion of a full process evaluation, the first full scale oxidation runs will be made. Table 5 shows the contemplated oxygen doping levels. The alloy oxygen tolerance comparison, at least at lower levels, will be made on the basis of equivalent atomic ppm. Intermediate doping levels of 200 ppm and 500 ppm will be run first, at which time the data may indicate that the proposed contamination levels should be changed.

The bend ductility data presented were obtained from samples intended primarily to establish oxidation rates and therefore represent a variety of oxygen levels. The observed average oxidation rates at 840°F in an oxygen partial pressure of  $76 \times 10^{-3}$  torr (76μ) are:

FS-85	$13.0 \times 10^{-6}$ g/cm <sup>2</sup> /hr
T-222	$6.6 \times 10^{-6}$ g/cm <sup>2</sup> /hr
T-111	$5.1 \times 10^{-6}$ g/cm <sup>2</sup> /hr

At the lower temperatures employed, (840°F) a surface oxide film is formed and the reaction rate is typically nonlinear in contrast to the linear rates observed at 1500°F.

**TABLE 5 - Selected Oxygen Contamination Levels**

Chronological Order	Level	Added O <sub>2</sub> (ppm) <sup>(1)</sup>		Total O <sub>2</sub> (ppm)		
		FS-85	T-111/T-222	FS-85	T-111	T-222
	As-Received			100	40	80
2	200	140	140	300	180	220
1	500	500	350	600	390	430
3 <sup>(2)</sup>	1000	1000	700	1100	740	780
4 <sup>(2)</sup>	2000	2000	1400	2100	1440	1480

(1) The contamination levels, expressed as ppm by weight, are adjusted to equivalent atomic ppm for each alloy.

(2) If indicated by initial data, other levels may be substituted.



The shielding effect of a carrier gas has been demonstrated at the 1500°F oxidation temperature where a comparison with other low partial pressure oxidation investigations was possible. Reported oxidation <sup>(5)</sup> rates of Cb-1Zr at 1600°F in vacuum with an oxygen partial pressure of  $1 \times 10^{-5}$  torr are comparable to oxidation rates we have measured on FS-85 using one atmosphere of helium doped with 100 ppm of oxygen, equivalent to an oxygen partial pressure of  $7.6 \times 10^{-2}$  torr. Thus, allowing for substantial differences in the oxidation rate of Cb-1Zr and FS-85, the carrier gas has produced equivalent reaction rates at oxygen partial pressures differing by several orders of magnitude.

#### IV. FUTURE WORK

Base line tensile properties at room and elevated temperatures will be obtained for the columbium and tantalum alloys in both the welded and unwelded conditions. Further information on the properties of plate welds will also be obtained.

The contaminated alloy weldability study will proceed with the first doping level, (500 ppm oxygen), of the three evaluation alloys, T-111, T-222, and FS-85.

## V. REFERENCES

1. R. A. Nadler, "Processing and Evaluation of Pre-Production Quantities of Columbium Alloy Sheet", Final Report, Bureau of Naval Weapons, Contract N600(19)-59546, Westinghouse Electric Corporation, Materials Manufacturing Division, January 20, 1964.
2. J. M. Gerken, and T. L. Fullerton, "Investigation of Weldability of Additional Columbium Alloys, TRW, Inc., ASD-TDR-63-843, October, 1963.
3. R. L. Ammon and A. M. Filippi, "Pilot Production and Evaluation of Tantalum Alloy Sheet", Ninth Quarterly Report, Contract NOw-64-0394-d.
4. W. L. Patton and J. Symonds, "Final Report on Refractory Alloy Foil Rolling Development Program", Technical Report NR. AFML-TR-65-43, Contract AF33(657)-8912, E. I. duPont de Nemours and Co., Inc. January 1965.
5. H. Inouye, The Contamination of Refractory Metals in Vacua Below  $10^{-6}$  Torr, AIME Symposium, Los Angeles, December 1963.
6. P. Kofstad, et al, High Temperature Oxidation of Niobium, ASTIA S1 Publ. No. 282, April 1960, WADC, Wright Field, Contract AF 61(052)-90.
7. W. D. Klopp, C. T. Sims, and R. I. Jaffee, Effects of Alloying on the Kinetics of Oxidation of Niobium, Second International Conference on the Peacetime Uses of Atomic Energy, Geneva, Switzerland, September, 1958.
8. R. W. Harrison, E. J. Delgrosso, "Low Pressure Oxidation of Columbium-1 Zirconium", Pratt & Whitney Aircraft - CANEL - Contract AT(30-1)-2789, April 30, 1964.
9. P. Kofstad, "Low Pressure Oxidation of Tantalum at 1300-1800°C", Journal of Less Common Metals, Vol. 7, 1964, Pgs 241-266.
10. R. Ogilvie, "Diffusion and Dispersed Phases in Refractory Metals", ASD-TDR-62-7.
11. R. A. Pasternak, "High Temperature Oxidation and Nitridation of Niobium in Ultra High Vacuum", Final Report - AEC Contract AT(04-3)-115 Stanford Research Institute, November 15, 1964.

DISTRIBUTION LIST

TRW  
Caldwell Research Center  
23555 Euclid Avenue  
Cleveland, Ohio, 44117  
Attn: Librarian  
G. J. Guarnieri

TRW  
New Devices Laboratories  
7209 Platt Avenue  
Cleveland, Ohio 44104  
Attn: Librarian

TRW  
Space Technology Laboratories  
One Space Park  
Redondo Beach, California  
Attn: Librarian

National Aeronautics & Space Adm.  
Washington, D. C. 20546  
Attn: Walter C. Scott  
James J. Lynch (RN)  
George C. Deutsch (RR)

National Aeronautics & Space Adm.  
Scientific & Technical Inf. Facility  
Box 5700  
Bethesda, Maryland 21811

National Aeronautics & Space Adm.  
Ames Research Center  
Moffet Field, California 94035  
Attn: Librarian

National Aeronautics & Space Adm.  
Goddard Space Flight Center  
Greenbelt, Maryland 20771  
Attn: Librarian

National Aeronautics & Space Adm.  
Langley Research Center  
Hampton, Virginia 23365  
Attn: Librarian

National Aeronautics & Space Adm.  
Manned Spacecraft Center  
Houston, Texas 77001  
Attn: Librarian

National Aeronautics & Space Adm.  
George C. Marshall Space Flight Center  
Huntsville, Alabama 35812  
Attn: Librarian  
Wm. A. Wilson R-ME-MM

National Aeronautics & Space Adm.  
Jet Propulsion Laboratory  
4800 Oak Grove Drive  
Pasadena, California 91103

National Aeronautics & Space Adm.  
21000 Brookpark Road  
Cleveland, Ohio 44135  
Attn: Librarian  
Dr. Bernard Lubarsky (SPSD)  
Roger Mather (NPTB)  
G. M. Ault  
Joe Joyce (NPTB)  
Paul Moorhead (NPTB)  
John J. Fackler (SPSPS)  
Norman T. Musial  
Thomas Strom  
T. A. Moss (NPTB)  
Dr. Louis Rosenblum  
John Creagh  
G. K. Watson  
Tom Moore  
George Tulsiak  
Report Control Section

DISTRIBUTION LIST  
(continued)

National Aeronautics & Space Adm.  
Western Operations Office  
150 Pico Boulevard  
Santa Monica, California 90406  
Attn: Mr. John Keeler

National Bureau of Standards  
Washington 25, D. C.  
Attn: Librarian

Aeronautical Systems Division  
Wright-Patterson Air Force Base  
Ohio  
Attn: Charles Armbruster (ASRPP-10)  
T. Cooper  
Librarian  
John L. Morris  
H. J. Middendorp (ASNRG)  
George Thompson (APIP-1)  
George Sherman (API)

Army Ordnance Frankford Arsenal  
Bridesburg Station  
Philadelphia 37, Pennsylvania  
Attn: Librarian

Bureau of Ships  
Dept. of the Navy  
Washington 25, D. C.  
Attn: Librarian

Bureau of Weapons  
Research and Engineering  
Material Division  
Washington 25, D. C.  
Attn: Librarian

U. S. Atomic Energy Commission  
Technical Reports Library  
Washington 25, D. C.  
Attn: J. M. O'Leary

U. S. Atomic Energy Commission  
P. O. Box 1102  
East Hartford, Connecticut  
Attn: C. E. McColley  
CANEL Project Office

U. S. Atomic Energy Commission  
Germantown, Maryland  
Attn: Col. E. L. Douthett  
SNAP 50/SPUR Project Office

H. Rothen  
SNAP 50/SPUR Project Office

Socrates Christopher

Major Gordon Dicker  
SNAP 50/SPUR Project Office

U. S. Atomic Energy Commission  
Technical Information Service Extension  
P. O. Box 62  
Oak Ridge, Tennessee

U. S. Atomic Energy Commission  
Washington 25, D. C.  
Attn: M. J. Whitman

Argonne National Laboratory  
9700 South Cross Avenue  
Argonne, Illinois  
Attn: Librarian

Brookhaven National Laboratory  
Upton, Long Island, New York  
Attn: Librarian

Oak Ridge National Laboratory  
Oak Ridge, Tennessee  
Attn: W. C. Thurber  
Dr. A. J. Miller  
Librarian

Office of Naval Research  
Power Division  
Washington 25, D. C.  
Attn: Librarian

U. S. Naval Research Laboratory  
Washington 25, D. C.  
Attn: Librarian

DISTRIBUTION LIST  
(continued)

Advanced Technology Laboratories  
Division of American Standard  
369 Whisman Road  
Mountain View, California  
Attn: Librarian

Aerojet General Corporation  
P. O. Box 296  
Azusa, California  
Attn: Librarian

Aerojet General Nucleonics  
P. O. Box 77  
San Ramon, California  
Attn: Librarian

AiResearch Manufacturing Co.  
Sky Harbor Airport  
402 South 36th Street  
Phoenix, Arizona  
Attn: Librarian  
E. A. Kovacevich  
John Dannan

AiResearch Manufacturing Co.  
9851-9951 Sepulveda Boulevard  
Los Angeles 45, California  
Attn: Librarian

I. I. T. Research Institute  
10 W. 35th Street  
Chicago, Illinois 60616

Atomics International  
8900 DeSoto Avenue  
Canoga Park, California

Avco  
Research & Advanced Development Dept.  
201 Lowell Street  
Wilmington, Massachusetts  
Attn: Librarian

Babcock and Wilcox Co.  
Research Center  
Alliance, Ohio  
Attn: Librarian

Battelle Memorial Institute  
505 King Avenue  
Columbus, Ohio  
Attn: C. M. Allen  
Librarian

The Bendix Corporation  
Research Laboratories Div.  
Southfield, Detroit 1, Michigan  
Attn: Librarian

The Boeing Company  
Seattle, Washington  
Attn: Librarian

Brush Beryllium Company  
Cleveland, Ohio  
Attn: Librarian

Carborundum Company  
Niagara Falls, New York  
Attn: Librarian

Chance Vought Aircraft, Inc.  
P. O. Box 5907  
Dallas 22, Texas  
Attn: Librarian

Clevite Corporation  
Mechanical Research Division  
540 East 105th Street  
Cleveland 8, Ohio  
Attn: Mr. N. C. Beerli  
Project Administrator

Climax Molybdenum Co. of Michigan  
Detroit, Michigan  
Attn: Librarian

Convair Astronautics  
5001 Kerrny Villa Road  
San Diego 11, California  
Attn: Librarian

E. I. duPont de Nemours & Co., Inc.  
Wilmington 98, Delaware  
Attn: Librarian

DISTRIBUTION LIST  
(continued)

Electro-Optical Systems, Inc.  
Advanced Power Systems Division  
Pasadena, California  
Attn: Librarian

Fansteel Metallurgical, Corp.  
North Chicago, Illinois  
Attn: Librarian

Ford Motor Company  
Aeronutronics  
Newport Beach, California  
Attn: Librarian

General Dynamics/General Atomic  
P. O. Box 608  
San Diego, California 92112  
Attn: Librarian

General Electric Company  
Atomic Power Equipment Div.  
P. O. Box 1131  
San Jose, California

General Electric Company  
Flight Propulsion Laboratory Dept.  
Cincinnati 15, Ohio  
Attn: Librarian

General Electric Company  
Missile and Space Vehicle Dept.  
3198 Chestnut Street  
Philadelphia 4, Pennsylvania  
Attn: Librarian

General Electric Company  
Vallecitos  
Vallecitos Atomic Lab.  
Pleasanton, California  
Attn: Librarian

General Electric Company  
Re-Entry Systems Dept.  
Cincinnati, Ohio  
Attn: Dr. J. W. Semmel

General Electric  
Lamp Metals & Components Dept.  
21800 Tungsten Road  
Cleveland, Ohio  
Attn: Librarian

General Dynamics/Fort Worth  
P. O. Box 748  
Fort Worth, Texas  
Attn: Librarian

General Motors Corp.  
Allison Division  
Indianapolis 6, Indiana  
Attn: Librarian

Hamilton Standard  
Div. of United Aircraft Corp.  
Windsor Locks, Connecticut  
Attn: Librarian

Hughes Aircraft Company  
Engineering Division  
Culver City, California  
Attn: Librarian

Lockheed Missiles and Space Div.  
Lockheed Aircraft Corp.  
Sunnyvale, California  
Attn: Librarian  
Mr. John N. Cox

Marquardt Aircraft Co.  
P. O. Box 2013  
Van Nuys, California  
Attn: Librarian

The Martin Company  
Baltimore 3, Maryland  
Attn: Librarian

The Martin Company  
Nuclear Division  
P. O. Box 5042  
Baltimore 20, Maryland  
Attn: Librarian

Martin Marietta Corp.  
Metals Technology Laboratory  
Wheeling, Illinois

Massachusetts Institute of Technology  
Cambridge 39, Massachusetts  
Attn: Librarian

DISTRIBUTION LIST  
(continued)

Materials Research & Development  
Manlabs, Inc.  
21 Erie Street  
Cambridge 39, Massachusetts

Materials Research Corp.  
Orangeburg, New York  
Attn: Librarian

McDonnell Aircraft  
St. Louis, Missouri  
Attn: Librarian

North American Aviation  
Los Angeles Division  
Los Angeles 9, California  
Attn: Librarian

Pratt & Whitney Aircraft  
400 Main Street  
East Hartford 8, Connecticut  
Attn: Librarian

Norton Company  
Worcester, Massachusetts  
Attn: Librarian

Pratt & Whitney  
Plant N  
North Haven, Connecticut  
Attn: Librarian

Pratt & Whitney Aircraft  
CANEL  
P. O. Box 611  
Middletown, Connecticut  
Attn: Librarian  
Dr. Robert Strouth

Republic Aviation Corporation  
Farmingdale, Long Island, New York  
Attn: Librarian

Solar  
2200 Pacific Highway  
San Diego 12, California  
Attn: Librarian

National Research Corp.  
45 Industrial Place  
Cambridge, Massachusetts  
Attn: R. W. Douglas

Southwest Research Institute  
8500 Culebra Road  
San Antonio 6, Texas  
Attn: Librarian

Rocketdyne  
Canoga Park, California  
Attn: Librarian

Superior Tube Company  
Norristown, Pennsylvania  
Attn: Mr. A. Bound

Sylvania Electric Products, Inc.  
Chem. & Metallurgical  
Towanda, Pennsylvania  
Attn: Librarian

Temescal Metallurgical  
Berkeley, California  
Attn: Librarian

Union Carbide Metals  
Niagara Falls, New York  
Attn: Librarian

Union Carbide Stellite Corp.  
Kokomo, Indiana  
Attn: Librarian

Union Carbide Nuclear Co.  
P. O. Box X  
Oak Ridge, Tennessee  
Attn: X-10 Laboratory Records Dept.

United Nuclear Corp.  
5 New Street  
White Plains, New York  
Attn: Librarian  
Mr. Albert Weinstein,  
Senior Engineer

Universal Cyclops Steel Corp.  
Refractomet Division  
Bridgeville, Pennsylvania  
Attn: C. P. Mueller

University of Michigan  
Department of Chemical & Metallurgical Eng.  
Ann Arbor, Michigan  
Attn: Librarian



DISTRIBUTION LIST  
(continued)

Vought Astronautics  
P. O. Box 5907  
Dallas 22, Texas  
Attn: Librarian

Wah Chang Corp.  
Albany, Oregon  
Attn: Librarian

Wolverine Tube Division  
Calumet & Hecla, Inc.  
17200 Southfield Road  
Allen Park, Michigan  
Attn: R. C. Cash

Wyman-Gordon Company  
North Grafton, Massachusetts  
Attn: Librarian